frontiers | Frontiers in Earth Science

TYPE Original Research
PUBLISHED 09 January 2025
DOI 10.3389/feart.2024.1525594

OPEN ACCESS

EDITED BY
Ramanathan Alagappan,
Jawaharlal Nehru University, India

REVIEWED BY
Zhongrui Wu,
RWTH Aachen University, Germany
Abdel-Aziz A. Abdel-Aziz,
Minia University, Egypt

*CORRESPONDENCE
Chuang Lei,
leichuang119@163.com

RECEIVED 10 November 2024
ACCEPTED 19 December 2024
PUBLISHED 09 January 2025

CITATION
Yin S, Yao A, Cheng J, Lei C, Wang Z, Zhang Z, Zhang Y, Wang Y, Han X and Ma Z (2025) Mineralogical and geochemical characteristics of the third member of Palaeogene Dongying formation in the Nanpu Sag, Bohai Bay Basin: implications for controlling on organic matter accumulation. *Front. Earth Sci.* 12:1525594. doi: 10.3389/feart.2024.1525594

Mineralogical and geochemical characteristics of the third member of Palaeogene Dongying formation in the Nanpu Sag, Bohai Bay Basin: implications for controlling on organic matter accumulation

Shiyan Yin[1,2], Aidong Yao[3], Jianzhong Cheng[4], Chuang Lei[2]*, Zhaosheng Wang[5], Zhenguo Zhang[5], Ying Zhang[2], Yu Wang[2], Xiaoying Han[2] and Zhigang Ma[6]

[1]Key Laboratory of Tectonics and Petroleum Resources, Ministry of Education, China University of Geosciences (Wuhan), Wuhan, China, [2]Collaborative Innovation Center of Green Development and Ecological Restoration of Mineral Resources, North China University of Science and Technology, Tangshan, China, [3]No. 6 Oil Production Plant of Daqing Oilfield Co. Ltd., Daqing, China, [4]Geological Research Institute of XDEC (logging Engineering Branch), Karamay, China, [5]Liaoning Key Laboratory of Green Development of Mineral Resources, Liaoning Technical University, Fuxin, China, [6]Inner Mongolia Linhe Yellow Rever National Wetland Park Management Center, Bayannur, China

Introduction and Methods: To identify the unconventional shale oil exploration potential of the third member of the Palaeogene Dongying Formation (Ed_3) in the Nanpu Sag, Bohai Bay Basin, variations in paleoclimate and paleoenvironment and their influence on organic matter accumulation were investigated through analyzing mineralogical and geochemical characteristics of forty-nine mudstone samples.

Results: Results show that the Ed_3 mudstones exhibit strong heterogeneity with the organic carbon content ranging from 0.30% to 2.66%, petroleum potential yield ranging from 0.44 to 11.41 mg/g, and hydrogen index ranging from 57 to 466 mg/g TOC, which are dominated by mixed kerogen and low maturity to maturity. Multiple mineralogical and geochemical proxies suggest that the semi-humid to semi-arid paleoclimate during the Ed_3 period governed the fluctuations of paleoenvironmental elements. From bottom to top, the paleowater depth varied in an order of shallow water, deep water, and shallow water, respectively, and the corresponding paleosalinity of brackish water, fresh water, and brackish waterr, respectively. Water column evolved from weak oxidation to weak reduction, and then to weak oxidation, respectively. Two development models of the Ed_3 mudstones under semi-humid to humid and semi-arid to arid climate were summarized based on the influence of paleoenvironmental elements on organic matter supply and preservation/degradation in sediments. Mudstones were deposited in a deep-water environment with high primary productivity under the semi-humid to humid climate. The mixed aquatic and terrigenous organic matte were efficiently preserved in stratified and reduced water columns, resulting in high organic

matter accumulation. Nevertheless, mudstones were developed in a shallow-water environment with medium primary productivity under the semi-arid to arid climate. Here, aquatic organic matter was oxidized and degraded in the oxidation condition, leading to low organic matter accumulation.

Discussion: The exploration of unconventional shale oil in the Ed_3 member of Nanpu Sag should focus on the organic-matter-rich mudstones developed in the humid climate.

KEYWORDS

Dongying formation, paleoclimate, paleoenvironment, organic matter accumulation, Nanpu Sag

1 Introduction

Organic matter accumulation in fine-grained sediments is a complex geological process influenced by multiple elements in the paleoenvironment, which are controlled by the co-evolution of tectonic and climatic factors (Carroll and Bohacs, 1999; 2001; Quan et al., 2017; Wang et al., 2020). It is achieved through the influence of paleoproductivity, paleowater depth, paleosalinity, and paleoredox conditions on the supply and preservation of organic matter. Paleoproductivity is an important factor affecting organic matter accumulation (Pedersen and Calvert, 1990). First, high primary productivity enhances the organic matter content in sediments. Second, the oxidation of excess organic matter can create anoxic conditions because of the consumption of free oxygen in the water column, which is conducive to the preservation of organic matter. Salinity leads to significant differences in the organic matter accumulation by governing the species and richness of planktonic organisms (Fu et al., 2022; Tang et al., 2020). Many euryhaline algae, e.g., cyanobacteria, diatoms, and green algae, etc., can survive in low-salinity water, whereas only a few salt-tolerant algae, e.g., amphora subacutiuscula, can thrive in high-salinity water. Nevertheless, organisms that are adapted to specific salinity ranges can propagate in these environments, benefiting from reduced competition for nutrients, survival space, and limited predators (Xu et al., 2024). Redox conditions play an important role in the preservation of hydrogen-rich organic matter. Water stratification controlled by the presence of salinity or temperature gradients can create an anoxic condition (Ocubalidet et al., 2018), particularly in deep-water environments. It is characterized by a lack of commutation between the surface oxygen-rich water and bottom oxygen-poor water at the stratification interface. Limited degradation of planktonic algae results in high organic matter accumulation. Nevertheless, a rapid commutation between the surface and bottom water can lead to oxic conditions with weak stratification, as seen in shallow-water environments (Lei et al., 2021b). Intense degradation by aerobic bacteria in the oxygen-enriched conditions could destroy algal organic matter during burial. Therefore, the reconstruction of paleolacustrine environments play an essential role in understanding the mechanisms of organic matter accumulation in fine-grained sediments. As carriers, fine-grained sediments record abundant information of paleoclimate and paleoenvironment in geological history. Recently, various methods have been developed to characterize the paleoclimate and paleoenvironment, including paleobiology, mineralogy, elemental geochemistry, organic geochemistry, and isotopic geochemistry, etc (Ghassal et al., 2018; Gyawali et al., 2019; Johnston et al., 2017; Moradi et al., 2016; Tribovillard et al., 2006; 2008; 2012; Yin et al., 2020; Wu et al., 2022).

In recent years, significant progress has been achieved in exploring and developing continental shale oil in major petroliferous basins in China, such as Songliao, Bohai Bay, Ordos, and Junggar basins. To reduce exploration uncertainties, increasing attention has been paid to the mechanisms of organic-matter-rich sediments (Cai et al., 2022; Wang et al., 2020; Wu et al., 2022; Zhang et al., 2017). Nanpu Sag has been recognized as an important petroliferous sag in the Bohai Bay Basin, with the conventional petroleum resources at approximately $7{,}000 \times 10^4$ t, and the unconventional petroleum resources at approximately $12{,}000 \times 10^4$ t (Jiang et al., 2023). Organic-matter-rich sediments in the Es_3, Es_1, and Ed_3 members are regarded as potential source rocks in the Nanpu Sag. Previous studies have suggested that the Es_3 and Es_1 members, with deep burial, high organic matter abundance, and Type I-II kerogen, are major source rocks in this sag. Owing to shallow burial and limited hydrocarbon generation capacity, less attention has been forced on the Ed_3 member in oil-gas exploration. Unexpectedly, unconventional shale oil has been discovered in the Ed_3 member of the Linque and Caofeidian sub-sags in the Nanpu Sag. No studies have concerned with the mechanisms of organic matter accumulation in the Ed_3 member, which hampered unconventional shale oil exploration.

In this study, a combination of mineralogy and geochemistry was used to interpret the paleoclimate and paleoenvironment of the Ed_3 member in the Nanpu Sag, and their influence on organic matter accumulation was discussed, providing insight into the shale oil exploration.

2 Geological setting

The Bohai Bay Basin is one of the major petroliferous basins in eastern China, with proven oil reserves of more than 150×10^8 t and proven natural gas reserves of more than 0.36×10^{12} m^3. It is situated in the east of North China Platform, and can be divided into six sub-basins, namely Liaohe, Bozhong, Jizhong, Huanghua, Jiyang, and Linqing (Figure 1A). The focus of this study, Nanpu Sag, is situated in the northeast of Huanghua sub-basin and close to the southern margin of the Yanshan fold belt, with an area of 1932 km^2. Based on the structural forms, it can be divided into eight secondary structural belts, i.e., Nanpu No.1, Nanpu No.2, Nanpu No.3, Nanpu

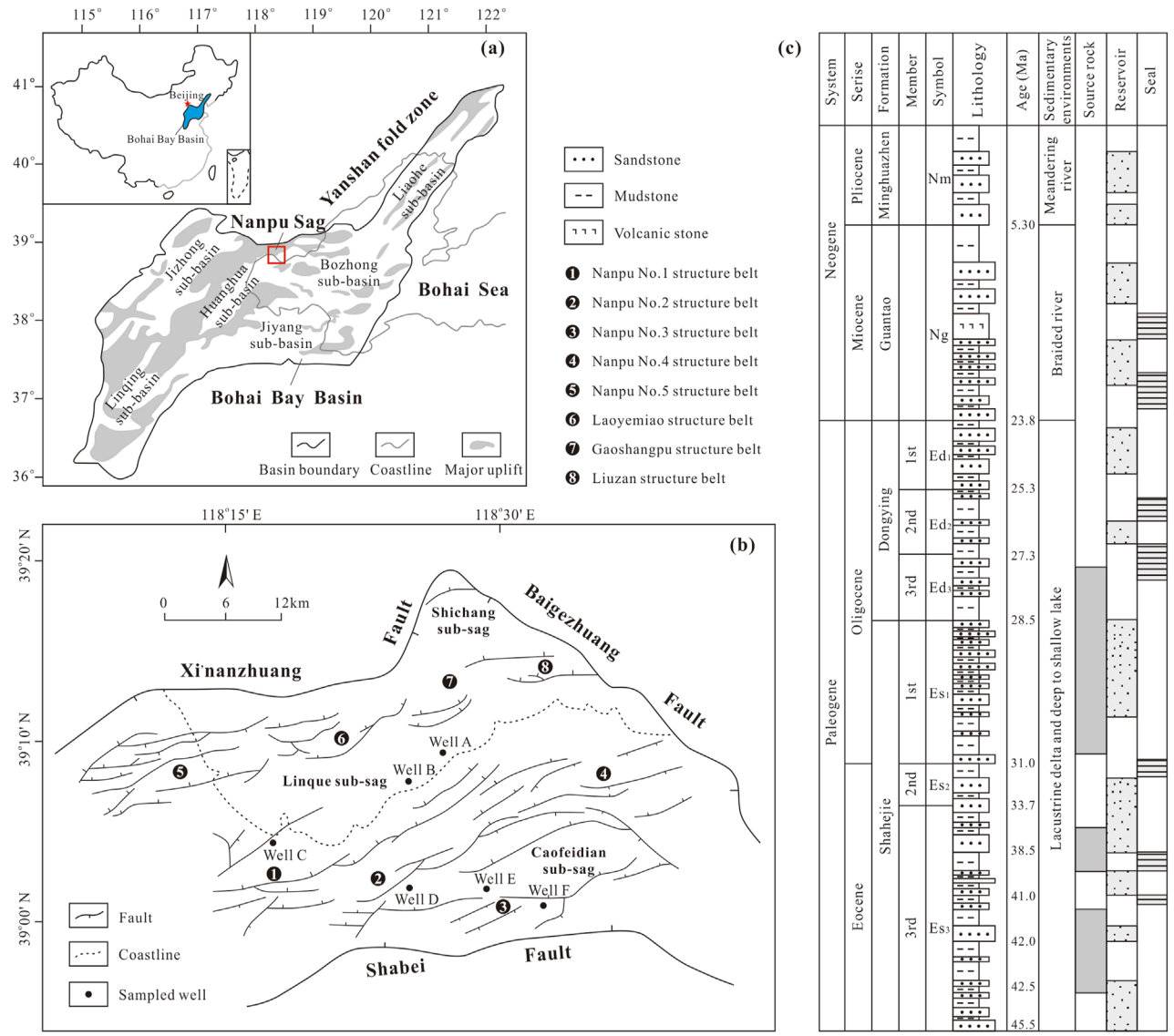

FIGURE 1
Regional structure **(A, B)** and stratigraphic comprehensive histogram **(C)** of the Nanpu Sag.

No.4, Nanpu No.5, Laoyemiao, Gaoshangpu and Liuzan, and three sub-sags, i.e., Shichang, Linque and Caofeidian (Figure 1B). The Nanpu Sag is a Cenozoic sedimentary basin developed on Mesozoic basement rocks, and exhibits faulting in the north and overlapping in the south. It is overlain by Cenozoic clastic sediments with a maximum thickness of 8,000 m, including Paleogene Shahejie (Es) and Dongying (Ed) formations, Neogene Guantao (Ng) and Minghuazhen (Nm) formations, and Quaternary Pingyuan (Qp) Formation (Figure 1C). Particularly, the Ed Formation can be divided into three members including Ed_3, Ed_2, and Ed_1, from bottom to top. The Ed_3 member, as the focus of this study, is an important source rock and oil-bearing reservoir in the Nanpu Sag. Controlled by the combination of strong activity of boundary faults and rapid subsidence of the basement, the deposition center of the Ed_3 member was located in the Linque and Caofeidian sub-sags, south of the Gaoliu fault. It is mainly composed of semi-deep/deep lake deposits. A series of fan delta sediments developed on the northern steep slope, and braided-river delta sediments developed on the southern gentle slope. Based on variations in lithological association, the Ed_3 member can be subdivided into two intervals including the lower interval (Ed_3l) and the upper interval (Ed_3u). The thickness of the Ed_3l interval is between 200 and 550 m, with a mud ratio of up to 70%, and the Ed_3u interval is between 180 and 450 m, with a mud ratio of up to 60%. Among these mudstones, colors are dominated by dark gray, black gray, and gray black, with the alternating micro-layered, layered and massive structures.

3 Materials and methods

In this study, two sample sets were taken from the Linque and Caofeidian sub-sags, because the deposition center of the Ed_3

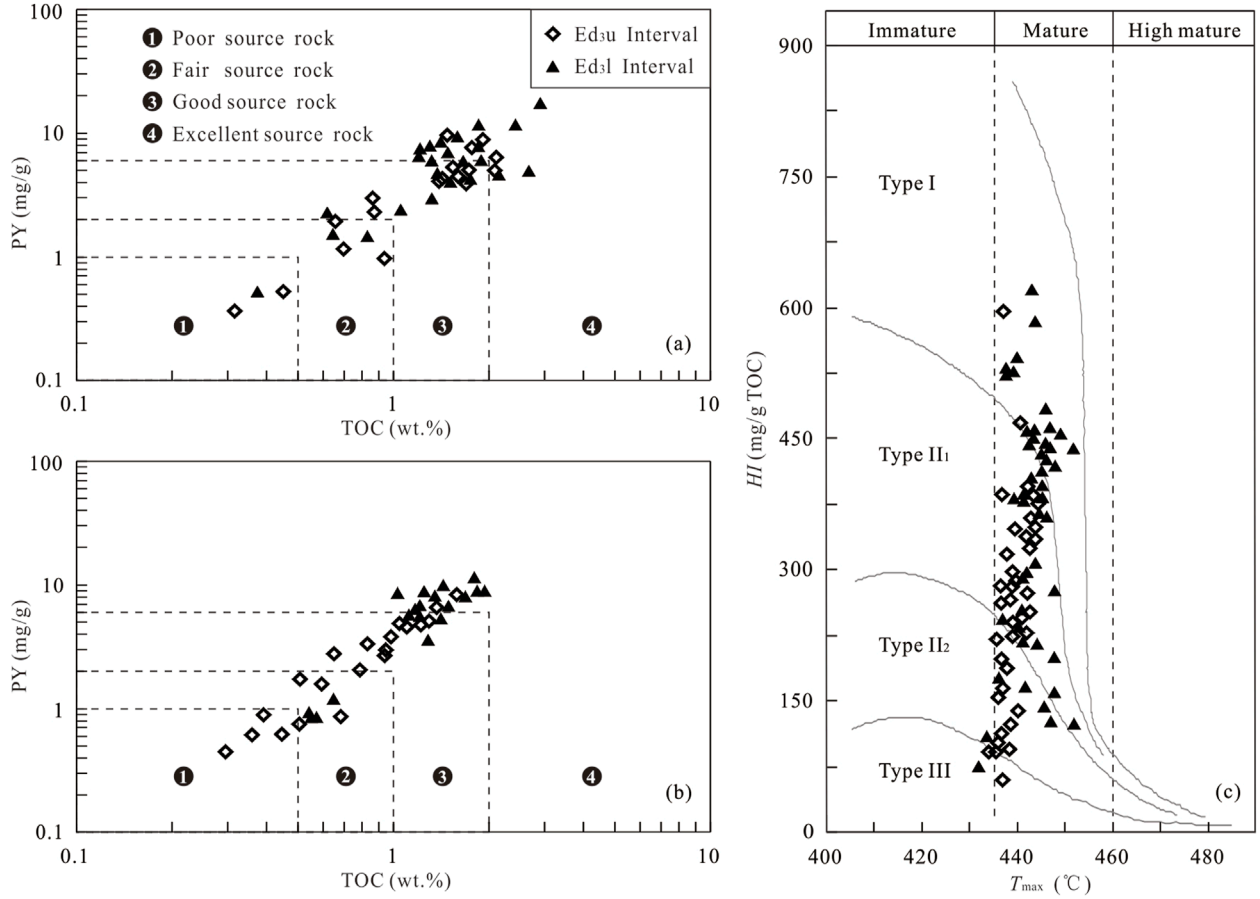

FIGURE 2
Organic matter abundance [**(A)** Linque sub-sag; **(B)** Caofeidian sub-sag] and type **(C)** of the Ed_3l and Ed_3u intervals in the Nanpu Sag. Note: Some data was collected from the PetroChina Jidong Oilfield Company.

member was located in these two sub-sags. One sample set includes forty-nine mudstone samples from six drilling wells (well location is shown in Figure 1B). It was employed for TOC and Rock–Eval pyrolysis analyses to estimate basic geochemical characteristics of source rocks. Another sample set includes twenty-one mudstone samples from Well E, which were selected for mineralogical component, major element, trace element, gas chromatography (GC), and gas chromatography-mass spectrometry (GC-MS) analysis to investigate the paleoclimate and paleoenvironment.

TOC and Rock-Eval pyrolysis parameters such as S_1, S_2, S_3, and T_{max} were conducted via a Rock-Eval II instrument furnished with total organic carbon measuring function. Mineralogical compositions were determined utilizing an X-ray diffractometer. Samples were crushed into a fine powder and then scanned from 5°C to 75°C at a rate of 2°C/min.

Major elements were determined using an X-ray fluorescence spectrometer. First, powder samples (less than 200 mesh) were dried in an oven at 105°C for 12 h. They were then heated at 1,000°C in a muddle furnace for 2 h. After cooling to 400°C, ashed samples were weighted, and the losses on ignition were recorded. Finally, these samples were mixed with lithium tetraborate and fused into glass beads for XRF analysis. Trace elements were determined using an Agilent 7500A inductively coupled plasma mass spectrometer (ICP-MS). First, powder samples were placed into mufflle furnace at 500°C to remove crystal water together with organic matter. The samples were sealed and dissolved with high-purity 0.1 mL HNO_3 and 0.1 mL HF in a Teflon beaker, and then heated at 190°C in an oven for 12 h. After cooling, the Teflon beaker was opened and heated at 140°C to achieve initial dryness before reacting with 1.0 mL HNO_3. Finally, the solution was transferred to a polyethylene bottle and diluted to a mixture (100 g) with 2% HNO_3 for analysis. The results were calibrated via standard and measured samples, with an analytical error of less than 5%.

Bitumen extractions were extracted from the powder samples using an azeotrope of methanol and methylene chloride (7:93) in a Soxhlet apparatus for 72 h. The fractions of hexane-soluble organic matter were separated into saturated components, aromatic components, and resin components through column chromatography. Saturated components were dissolved in hexane and analyzed by GC (a PONA fused silica column, 60 m × 0.25 mm i. d., film thickness 0.25 μm, with the temperature programmed from 40°C to 300°C at a rate of 4°C/min, and then held at 300°C for 30 min). GC–MS experiments were executed on an Agilent 7890A-GC/5975C-MS instrument coupled with a HP-5MS fused silica column (30 m × 0.25 mm i. d., film thickness 0.25 μm). For biomarkers analysis, the fragmentograms of steroids (m/z

10.3389/feart.2024.1525594

TABLE 1 Bulk compositions of the Ed_3l and Ed_3u intervals in the Nanpu Sag.

SN	Wells	Depth (m)	Interval	TOC	Rock-Eval pyrolysis					
					S_1	S_2	T_{max}	HI	PI	PY
1	Well E	3720	Ed_3u	0.45	0.02	0.50	437	111	0.04	0.52
2	Well E	3747	Ed_3u	0.69	0.03	1.10	437	159	0.03	1.13
3	Well E	3760	Ed_3u	0.94	0.03	0.94	436	100	0.03	0.97
4	Well E	3785	Ed_3u	1.66	0.15	3.99	440	240	0.04	4.14
5	Well E	3867	Ed_3u	1.58	0.19	4.58	440	290	0.04	4.77
6	Well E	3880	Ed_3u	1.39	0.20	3.91	438	281	0.05	4.11
7	Well E	3920	Ed_3u	1.40	0.19	4.13	439	295	0.04	4.32
8	Well E	3965	Ed_3u	1.91	1.26	7.41	442	388	0.15	8.67
9	Well E	3975	Ed_3u	1.78	0.81	6.74	444	379	0.11	7.55
10	Well E	4060	Ed_3l	1.31	0.04	2.85	441	218	0.01	2.89
11	Well E	4070	Ed_3l	1.71	0.28	3.98	440	233	0.07	4.26
12	Well E	4083	Ed_3l	1.86	0.36	5.48	442	295	0.06	5.84
13	Well E	4090.2	Ed_3l	1.83	0.78	6.89	442	377	0.10	7.67
14	Well E	4092.5	Ed_3l	2.41	1.20	10.21	446	424	0.11	11.41
15	Well E	4100	Ed_3l	1.67	0.43	5.11	444	306	0.08	5.54
16	Well E	4120	Ed_3l	1.51	0.26	3.79	441	251	0.06	4.05
17	Well E	4170	Ed_3l	2.66	0.48	4.33	442	163	0.10	4.81
18	Well E	4215.5	Ed_3l	0.64	0.13	1.36	444	213	0.09	1.49
19	Well E	4216.3	Ed_3l	1.38	0.63	3.77	448	273	0.14	4.40
20	Well E	4218.7	Ed_3l	0.82	0.13	1.28	448	156	0.09	1.41
21	Well E	4219.5	Ed_3l	1.05	0.22	2.06	448	196	0.10	2.28
22	Well D	3591.6	Ed_3u	0.30	0.27	0.17	437	57	0.61	0.44
23	Well D	3592.5	Ed_3u	0.69	0.46	0.40	437	58	0.53	0.86
24	Well D	3617.6	Ed_3u	0.65	0.41	2.25	440	344	0.15	2.66
25	Well D	3618.6	Ed_3u	0.99	0.39	3.32	442	334	0.11	3.71
26	Well D	3619.2	Ed_3u	1.60	0.65	7.46	441	466	0.08	8.11
27	Well F	4859.7	Ed_3u	1.05	1.39	3.41	443	323	0.29	4.80
28	Well F	4862.6	Ed_3u	1.38	1.74	4.81	444	349	0.27	6.55
29	Well B	3793	Ed_3u	0.79	0.55	1.46	438	186	0.27	2.01
30	Well B	3824	Ed_3u	0.39	0.26	0.60	436	153	0.3	0.86
31	Well B	3917	Ed_3u	0.51	0.56	1.12	439	222	0.33	1.68

(Continued on the following page)

10.3389/feart.2024.1525594

TABLE 1 (*Continued*) Bulk compositions of the Ed_3l and Ed_3u intervals in the Nanpu Sag.

SN	Wells	Depth (m)	Interval	TOC	Rock-Eval pyrolysis					
					S_1	S_2	T_{max}	HI	PI	PY
32	Well B	3912	Ed_3u	0.84	0.47	2.81	444	336	0.14	3.28
33	Well B	3946	Ed_3u	0.61	0.34	1.18	437	195	0.22	1.52
34	Well B	3936	Ed_3u	1.11	0.64	3.85	444	347	0.14	4.49
35	Well B	3974	Ed_3u	0.95	0.44	2.36	443	249	0.16	2.8
36	Well B	4007	Ed_3u	1.23	0.39	4.41	443	358	0.08	4.8
37	Well C	4195.3	Ed_3l	1.17	0.95	5.04	445	430	0.16	5.99
38	Well C	4196.2	Ed_3l	1.12	1.07	4.39	445	391	0.2	5.46
39	Well C	4197.3	Ed_3l	1.09	0.91	4.30	445	395	0.17	5.21
40	Well C	4198.3	Ed_3l	1.32	0.92	5.87	445	443	0.14	6.79
41	Well C	4199.3	Ed_3l	1.38	1.58	6.05	445	439	0.21	7.63
42	Well C	4200.9	Ed_3l	1.28	1.47	5.74	444	449	0.2	7.21
43	Well C	4201.3	Ed_3l	1.16	1.15	4.82	448	414	0.19	5.97
44	Well C	4202.8	Ed_3l	1.37	1.52	6.32	447	461	0.19	7.84
45	Well A	4501.5	Ed_3l	1.93	1.10	7.33	439	380	0.13	8.43
46	Well A	4502.5	Ed_3l	1.28	0.37	3.08	437	241	0.11	3.45
47	Well A	4503.3	Ed_3l	1.72	1.06	6.55	441	385	0.14	7.61
48	Well A	4506.6	Ed_3l	1.82	0.50	8.08	443	444	0.06	8.58
49	Well A	4507.1	Ed_3l	1.49	0.54	5.97	443	401	0.08	6.51

Note: TOC, total organic carbon, %.
S_1, free hydrocarbon content, mg/g.
S_2, remaining hydrocarbon generative potential, mg/g.
T_{max}, Temperature at the maximum of S_2 peak, °C.
HI, Hydrogen index (S_2/TOC × 100), mg/g TOC.
PI, Production index [$S_1/(S_1+S_2)$].
PY, Petroleum potential yield (S_1+S_2), mg/g.

= 217) and terpenoids (m/z = 191) were recorded. Individual components were identified by comparing their retention times and mass spectra with published data. The relative abundances of steroids and terpenoids were calculated by determining peak heights in the m/z = 191 and m/z = 217 fragmentograms, respectively.

4 Results

4.1 Basic geochemical characteristics of source rocks

Owing to the rapid change in the deposition environment, the Ed_3 mudstones exhibit strong heterogeneity, especially in terms of organic matter abundance, type, and hydrocarbon-generation potential (Figure 2). Based on geochemical data analysis (Table 1), the Ed_3l interval was in a range of 0.64%–2.66% in TOC, with a mean of 1.48%, and in a range of 1.41–11.41 mg/g in PY, with a mean of 5.71 mg/g, indicating high-quality source rocks. The Ed_3u interval was 0.30%–1.91% in TOC, with a mean of 1.08%, and 0.44–8.67 mg/g in PY, with a mean of 3.78 mg/g, indicating general-quality source rocks. Generally, hydrogen index (HI) > 400 mg/g TOC, 150–400 mg/g TOC, 50–150 mg/g TOC suggests oil-prone kerogen (Type-I), mixed kerogen (Type-II), and gas-prone kerogen (Type-III), respectively. HI values of the Ed_3l and Ed_3u intervals were 156–461 mg/g TOC and 57–466 mg/g TOC, respectively, indicating that they were dominated by type II kerogen with a certain proportion of Type I and III kerogen. T_{max} can serve as an effective proxy for evaluating thermal maturity

TABLE 2 Mineralogical compositions of the Ed_3l and Ed_3u intervals in the Nanpu Sag.

SN	Depth (m)	Interval	Mineral components (wt.%)						
			Quartz	Feldspar	Calcite	Dolomite	Clay minerals	Pyrite	Halite
1	3720	Ed_3u	41.6	13.3	8.5	7.6	28.0	0	1.0
2	3747	Ed_3u	46.2	18.1	9.5	9.2	17.0	0	0
3	3760	Ed_3u	38.6	8.7	8.2	9.0	30.9	0	3.6
4	3785	Ed_3u	35.2	13.0	11.7	7.7	30.9	0	1.5
5	3867	Ed_3u	37.2	11.8	13.4	5.0	30.6	0	2
6	3880	Ed_3u	43.5	11.2	13.7	10.1	21.5	0	0
7	3920	Ed_3u	36.0	11.1	13.1	5.4	33.2	0	1.2
8	3965	Ed_3u	44.3	24.5	7.1	4.6	19.5	0	0
9	3975	Ed_3u	42.5	23.5	6.4	6.1	21.5	0	0
10	4060	Ed_3l	37.8	20.1	5.5	5.1	31.5	0	0
11	4070	Ed_3l	40.4	10.4	6.6	3.6	37.4	1.6	0
12	4083	Ed_3l	37.4	13.0	6.6	5.0	35.7	2.3	0
13	4090.2	Ed_3l	39.8	12.7	6.1	5.4	34.1	1.9	0
14	4092.5	Ed_3l	44.5	13.8	5.0	3.3	31.4	2.0	0
15	4100	Ed_3l	44.1	7.7	7.6	4.7	35.9	0	0
16	4120	Ed_3l	34.4	11.6	7.2	10.6	36.2	0	0
17	4170	Ed_3l	39.4	9.8	8.3	5.5	34.3	2.7	0
18	4215.5	Ed_3l	35.5	15.1	12.0	4.0	33.4	0	0
19	4216.3	Ed_3l	40.7	9.8	9.6	6.5	31.1	2.3	0
20	4218.7	Ed_3l	36.7	7.3	9.4	5.2	40.1	1.3	0
21	4219.5	Ed_3l	43.4	8.1	10.4	6.4	30.5	1.2	0

(Bechtel et al., 2012). T_{max} values for immature, low mature, mature, high mature and overmature organic matter are <435°C, 435°C–445°C, 445°C–455°C, 455°C–490°C, >490°C, respectively. The Ed_3l and Ed_3u intervals had a narrow T_{max} ranging from 440°C to 448°C and 436°C–444°C, respectively. It suggests that the thermal maturity of the analyzed samples varies between just pre-oil window and mid-oil window thermogenic conditions for hydrocarbon generation. Note that in Figures 2A, B, the Ed_3 source rocks developed in the deposition centers of the Nanpu Sag, namely Linque sub-sag and Caofeidian sub-sag, are comparable.

4.2 Mineralogical components

The mineralogical components identified in the Ed_3 member include quartz, feldspar, calcite, dolomite, clay minerals, and a small amount of pyrite and halite (Table 2). Quartz and clay minerals were the dominant mineral components (Figure 3), varying between 34.4 wt.% and 46.2 wt.% (average 39.9 wt.%), 17.0 wt.% and 40.1 wt.% (average 30.7 wt.%), respectively. The contents of feldspar, calcite, and dolomite were in a range of 7.3–24.5 wt.%, 5.0–13.7 wt.%, and 3.3–10.6 wt.%, respectively, with means of 13.1 wt.%, 8.8 wt.%, and 6.2 wt.%, respectively. A low content of pyrite was only found in the Ed_3l interval ranged from 0 to 2.7 wt.% (average 1.2 wt.%), and halite was only found in the Ed_3u interval ranged from 0 to 3.6 wt.% (average1.0 wt.%).

4.3 Major and trace elements

The major element measurements are shown in Table 3. Major elements such as SiO_2 (53.94%–63.72%), Al_2O_3

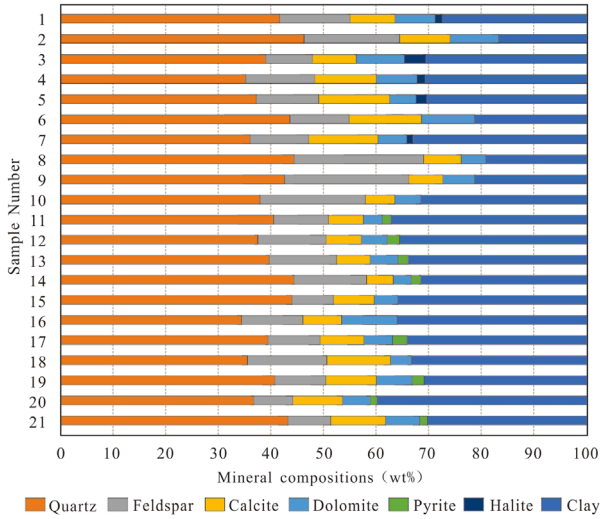

FIGURE 3
Mineralogical compositions of the Ed_3l and Ed_3u intervals in the Nanpu Sag.

(12.56%–14.98%),TFe_2O_3 (4.62%–8.06%), CaO (2.74%–9.23%), MgO (2.09%–3.74%), Na_2O (1.36%–4.43%), K_2O (2.01%–2.94%), and TiO_2 (0.64%–2.26%) showed significant vertical fluctuations. Terrigenous detrital, authigenic, and hydrothermal components are the main sources of major and trace elements in sediments (Tripathy et al., 2014; Xu et al., 2012). Al_2O_3 is chemically stable and little affected by weathering and diagenesis in late stage (Tribovillard et al., 2006). It is widely applied to estimate terrigenous debris influx. Results show that the Al_2O_3 concentrations in the Ed_3l and Ed_3u intervals were 13.13%–14.72% and 12.56%–14.08%, respectively, which were lower than that in the PAAS (18.90%). Hence, it is preliminarily concluded that these sediments were relatively poor in terrigenous detrital components and rich in authigenic or hydrothermal components. CaO primarily occurrs in carbonate minerals. The CaO concentrations in the Ed_3l and Ed_3u intervals fluctuated within the range of 2.74%–7.81% and 5.60%–9.23%, respectively. From the Ed_3l interval to the Ed_3u interval, the CaO concentration showed a trend of decreasing first and then increasing.

The trace element measurements are shown in Table 4. The concentrations of most trace elements were lower than 100×10^{-6}, except for Ba (785×10^{-6}–2151×10^{-6}), Mn (462.3×10^{-6}–979.6×10^{-6}), Sr (257.9×10^{-6}–430.2×10^{-6}), and Zn (369.6×10^{-6}–4911.0×10^{-6}). There was no significant correlation between trace elements and Al_2O_3 in the analyzed samples (not shown), indicating that the change in trace element concentration was not governed by detrital flux. The enrichment factor (EF), expressed as $(Element/Al)_{sample}/(Element/Al)_{PAAS}$, can be applied to investigate the variation in trace element concentrations in parent material after weathering, sedimentation, and diagenesis (Algeo and Tribovillard, 2009; Garzanti et al., 2015; Tribovillard et al., 2006; 2008). Dai et al. (2015) classified the enrichment or depletion of trace elements into six levels: depleted ($EF \leq 0.5$), normal ($0.5 < EF \leq 2$), slightly enriched ($2 < EF \leq 5$), enriched ($5 < EF \leq 10$), significantly enriched ($10 < EF \leq 100$), and unusually enriched ($EF > 100$). Results show that some trace elements in the Ed_3l and Ed_3u intervals displayed differential enrichment, e.g., Ba and Sr were slightly enriched with EF between 2.1 and 4.2, and Zn was enriched or significantly enriched with EF between 6.1 and 38.7. The remaining trace elements were close to those in the PAAS with the EF of 0.5–1.7 (Figure 4).

Diagenetic alteration can cause the enrichment of Mn and the depletion of Sr in sediments, with the corresponding Mn/Sr ratio more than 10 (Kaufman and Knoll, 1995). Results show that the Mn/Sr ratios of the Ed_3l and Ed_3u intervals varied between 1.2 and 2.0, suggesting that the trace element concentrations were not affected by diagenetic alteration. Morford et al. (2005) proposed that hydrothermal fluid would enhance the abundance of Fe and Mn in sediments. And the concentrations of both V and Mo are significantly altered because of their involvement in the Mn cycle. No hydrothermal fluid was observed in the Oligocene strata as well as in the overlying strata in Well E. In addition, all samples in the Al-Fe-Mn triangular diagram fall into the non-hydrothermal zone (Figure 5), excluding the influence of hydrothermal fluid on the variation in trace element concentrations. Therefore, the measurements of these samples are in response to the original sedimentary environment and can be applied to investigate the paleoclimate and paleoenvironment.

4.4 Biomarkers

4.4.1 *n*-alkanes and isoprenoids

The identified *n*-alkanes in the Ed_3l and Ed_3u intervals were dominated by nC_{12}-nC_{35}, with the max peak at nC_{21} or nC_{23}. The distribution pattern of *n*-alkanes is an effective indicator for deciphering original organic matter origin (Sachsenhofer et al., 2017; Volkman et al., 1990). Low-carbon compositions ($<nC_{20}$) dominated in *n*-alkanes derive from algae and microorganisms, and high-carbon compositions ($>nC_{25}$) dominated in *n*-alkanes originate from terrigenous higher plants. The distribution of *n*-alkanes in the Ed_3l and Ed_3u intervals was unimodal (Figure 6), where the abundance of low-carbon and high-carbon compositions was similar (C_{21}^-/C_{22}^+ = 0.78–1.43, Table 5), indicating the mixed origin of aquatic and terrigenous organic matter. Affected by low maturity, the Ed_3l and Ed_3u intervals had high CPI values of 1.08–1.24 and 1.27–1.50, respectively, and high OEP values of 1.03–1.15 and 1.16–1.35, respectively.

Pristane (Pr) and phytane (Ph) are the most common acyclic isoprenoids in source rocks. These two compounds are primarily derived from phytol, which is present in the side chain of chlorophyll. It is achieved under specific redox conditions (Peters et al., 2005a). Phytanol is preferentially oxidized to phytanic acid under oxidation conditions, and then produces pristane via the removal of ethanol. In contrast, phytanol is transformed into dihydrophytol through hydrogenation under reduction conditions, and subsequently produces phytane via hydrogenation and the removal of ethanol. The abundance of Pr and Ph in the analyzed samples was lower than that of adjacent *n*-alkanes, with both Pr/nC_{17} and Ph/nC_{18} values less than 1.0 (Figure 7A). Additionally, the abundance of Pr in the Ed_3l and Ed_3u intervals was higher than that

TABLE 3 Major element concentrations of the Ed_3l and Ed_3u intervals in the Nanpu Sag.

SN	Depth (m)	Interval	TOC (wt%)	Major element concentrations (%)							
				SiO_2	Al_2O_3	TFe_2O_3	CaO	MgO	Na_2O	K_2O	TiO_2
1	3720	Ed_3u	0.45	55.46	13.89	5.07	5.60	2.20	1.52	2.67	0.72
2	3747	Ed_3u	0.69	60.07	13.22	4.62	6.52	2.16	1.40	2.82	0.69
3	3760	Ed_3u	0.94	56.66	12.84	4.71	6.58	2.17	1.43	2.60	0.67
4	3785	Ed_3u	1.66	57.79	12.56	4.66	9.23	2.22	1.36	2.59	0.64
5	3867	Ed_3u	1.58	53.94	13.26	4.81	7.31	2.19	1.42	2.47	0.64
6	3880	Ed_3u	1.39	59.12	13.66	4.80	5.61	2.09	1.54	2.57	0.67
7	3920	Ed_3u	1.40	58.16	14.08	5.05	6.73	2.25	1.42	2.71	0.69
8	3965	Ed_3u	1.91	58.16	13.83	4.83	6.20	2.09	1.46	2.84	0.69
9	3975	Ed_3u	1.78	59.59	13.16	4.63	5.92	2.14	1.62	2.33	0.73
10	4060	Ed_3l	1.31	58.49	14.61	5.50	3.86	2.27	2.97	2.59	0.88
11	4070	Ed_3l	1.71	60.21	14.06	5.27	4.70	2.11	2.40	2.64	0.86
12	4083	Ed_3l	1.86	58.70	14.70	5.43	3.87	2.19	3.81	2.70	0.88
13	4090.2	Ed_3l	1.83	62.92	14.72	5.34	3.17	2.26	4.04	2.94	0.86
14	4092.5	Ed_3l	2.41	59.38	14.51	5.20	3.74	2.29	3.50	2.78	0.84
15	4100	Ed_3l	1.67	61.51	14.69	5.38	2.92	2.25	4.03	2.62	0.88
16	4120	Ed_3l	1.51	59.66	14.61	4.90	2.74	2.18	4.43	2.87	0.88
17	4170	Ed_3l	2.66	60.47	14.22	4.87	3.67	2.20	3.59	2.37	0.87
18	4215.5	Ed_3l	0.64	62.68	14.95	7.50	7.33	3.74	3.02	2.18	1.95
19	4216.3	Ed_3l	1.38	62.45	14.53	8.06	7.81	3.25	3.28	2.01	2.26
20	4218.7	Ed_3l	0.82	58.32	14.98	5.45	4.18	2.24	3.61	2.61	1.03
21	4219.5	Ed_3l	1.05	63.72	14.92	7.71	7.44	3.03	3.20	2.38	1.94
PAAS				62.80	18.90	7.22	1.30	2.20	1.20	2.20	1.00

Note: PAAS, is the component of the Post-Archean Australian Shale published by Taylor and McLennan (1985).

of Ph, with Pr/Ph values ranging from 1.48 to 3.29 and 1.92 to 4.41, respectively.

4.4.2 Steroids

Considerable steroid compounds such as pregnane, regular sterane, and diasterane were identified from m/z = 217 ion chromatograms (Figure 6). Regular steranes hold considerable biogenic significance (Farhaduzzaman et al., 2012; Peters et al., 2005b), e.g., C_{27} regular steranes are mainly originated from aquatic organisms, C_{28} regular steranes are derived from chlorophyll-c containing phytoplankton, and C_{29} regular steranes are primarily sourced from terrigenous higher plants. The relative abundances of C_{27}, C_{28}, C_{29} regular steranes in the Ed_3l and Ed_3u intervals ranged from 32.5% to 44.4%, 18.8%–31.4%, 31.1%–46.3% and 26.5%–38.3%, 20.5%–30.0%, 38.2%–51.1%, respectively. The typical "V" shape observed in the Figure 6 also suggests a mixed origin of aquatic and terrigenous organic matter.

There are four common configurations of regular steranes, including ααα20R, ααα20S, αββ20R, and αββ20S. Increasing thermal maturity can transform unstable αα configuration into stable ββ configuration, as well as convert unstable "R" shape into stable "S" shape (Hanson et al., 2000). Consequently, the ratios of C_{29} sterane ββ/(αα + ββ) and C_{29} sterane 20S/(S + R) are expected to increase with increasing thermal maturity, with determined thermodynamic equilibrium mixtures at 0.67–0.71 and 0.52–0.55, respectively. The isomerization of steranes in the Ed_3l and Ed_3u

TABLE 4 Trace element concentrations of the Ed_3l and Ed_3u intervals in the Nanpu Sag.

SN	Depth (m)	Interval	Trace element concentrations (10^{-6})										
			Ba	Cd	Cr	Ga	Mn	Ni	Sr	V	Zn	Co	Pb
1	3720	Ed_3u	2103	0.28	88.24	14.67	546.00	36.53	279.50	75.35	369.60	15.54	24.11
2	3747	Ed_3u	1,224	0.25	72.87	13.91	567.80	31.82	277.40	71.36	1857.00	20.83	21.59
3	3760	Ed_3u	1,377	0.26	75.12	14.69	542.90	33.08	297.80	70.52	2163.00	21.72	22.17
4	3785	Ed_3u	1,194	0.25	78.13	16.90	534.90	32.48	361.50	65.49	1,082.00	15.34	21.84
5	3867	Ed_3u	1,664	0.27	76.51	14.93	536.00	34.61	333.60	64.92	408.50	17.00	22.76
6	3880	Ed_3u	1856	0.27	77.69	13.21	502.70	34.25	273.10	67.61	535.20	15.05	22.65
7	3920	Ed_3u	835	0.28	94.17	15.09	476.20	36.79	290.90	68.98	1,279.00	21.84	23.87
8	3965	Ed_3u	785	0.27	73.86	14.40	496.90	35.09	274.20	68.76	516.90	14.65	22.72
9	3975	Ed_3u	1,400	0.24	78.53	14.00	462.30	31.49	281.80	77.43	1,098.00	19.11	21.67
10	4060	Ed_3l	2132	0.31	89.75	10.61	639.30	40.15	319.30	94.30	675.00	19.25	25.19
11	4070	Ed_3l	1897	0.30	87.70	12.29	600.20	37.07	308.90	91.41	623.90	18.91	23.95
12	4083	Ed_3l	1837	0.31	85.31	10.48	584.00	38.48	320.00	94.56	818.10	21.62	24.77
13	4090.2	Ed_3l	1775	0.30	91.37	10.54	656.60	38.16	294.00	91.65	816.50	16.44	25.49
14	4092.5	Ed_3l	1735	0.29	85.84	11.32	586.30	36.45	290.20	89.05	643.00	15.58	24.74
15	4100	Ed_3l	2102	0.30	89.20	10.18	780.80	38.62	286.20	93.67	537.50	16.59	25.80
16	4120	Ed_3l	1856	0.28	80.27	9.63	562.30	35.22	257.90	94.27	2547.00	20.58	23.46
17	4170	Ed_3l	1,298	0.28	85.32	10.56	712.10	34.61	265.80	93.28	593.80	12.95	23.34
18	4215.5	Ed_3l	1,003	0.44	106.00	17.16	914.50	54.63	429.10	221.90	4911.00	42.14	36.57
19	4216.3	Ed_3l	800	0.48	85.00	18.55	979.60	59.07	430.20	254.70	1,023.00	32.42	39.56
20	4218.7	Ed_3l	2151	0.32	86.33	12.33	577.10	39.86	310.90	109.40	745.20	18.93	26.42
21	4219.5	Ed_3l	1,149	0.46	93.19	18.06	938.20	56.70	401.00	222.10	1,285.00	29.61	37.74
PAAS			650.00	—	110.00	17.00	847.00	55.00	200.00	1.00	150.00	23.00	20.00

intervals was weak, with the C_{29} sterane ββ/(αα + ββ) ratio of 0.52–0.67 and 0.40–0.57 (Figure 7B), respectively, and the C_{29} sterane 20S/(S + R) ratio of 0.36–0.41 and 0.27–0.44, respectively. These suggest that the Ed_3l and Ed_3u intervals is present in low-mature to mature stage.

4.4.3 Terpenoids

Considerable terpenoid compounds including tricyclic terpane, tetracyclic terpane, and pentacyclic triterpene such as C_{27} norneohopane (Ts), C_{27} norhopane (Tm), C_{29} norhopane, C_{29} norneohopane, C_{30} hopane, C_{31}-C_{35} homohopane, and gammacerane were identified from m/z = 191 ion chromatograms (Figure 6). The Ts/Tm ratios of the Ed_3l and Ed_3u intervals varied in the range of 0.74–4.81 and 0.25–1.20, respectively, which can effectively distinguish hydrocarbon generation products. The C_{29} Ts/C_{29} hopane ratios of the Ed_3l and Ed_3u intervals ranged between 0.37–1.49 and 0.16–0.54 (Figure 7C), respectively. The abundance of C_{30} hopane was higher than that of C_{29} norhopane in the Ed_3l and Ed_3u intervals, with the C_{29}/C_{30} hopane ratios of 0.16–0.45 and 0.32–0.99 (Figure 7D), respectively. The relative abundance of C_{31}-C_{35} homohopane represented a positive sequence, i.e., C_{31} homohopane > C_{32} homohopane > C_{33} homohopane > C_{34} homohopane > C_{35} homohopane, especially the abundance of C_{34} and C_{35} homohopane was extremely low, which is consistent with the non-strong reducing sedimentary environment (Peters and Moldowan, 1991).

Gammacerane, an important biomarker, is derived from the reduction of tetrahymanol (Ten Haven et al., 1989). The principal

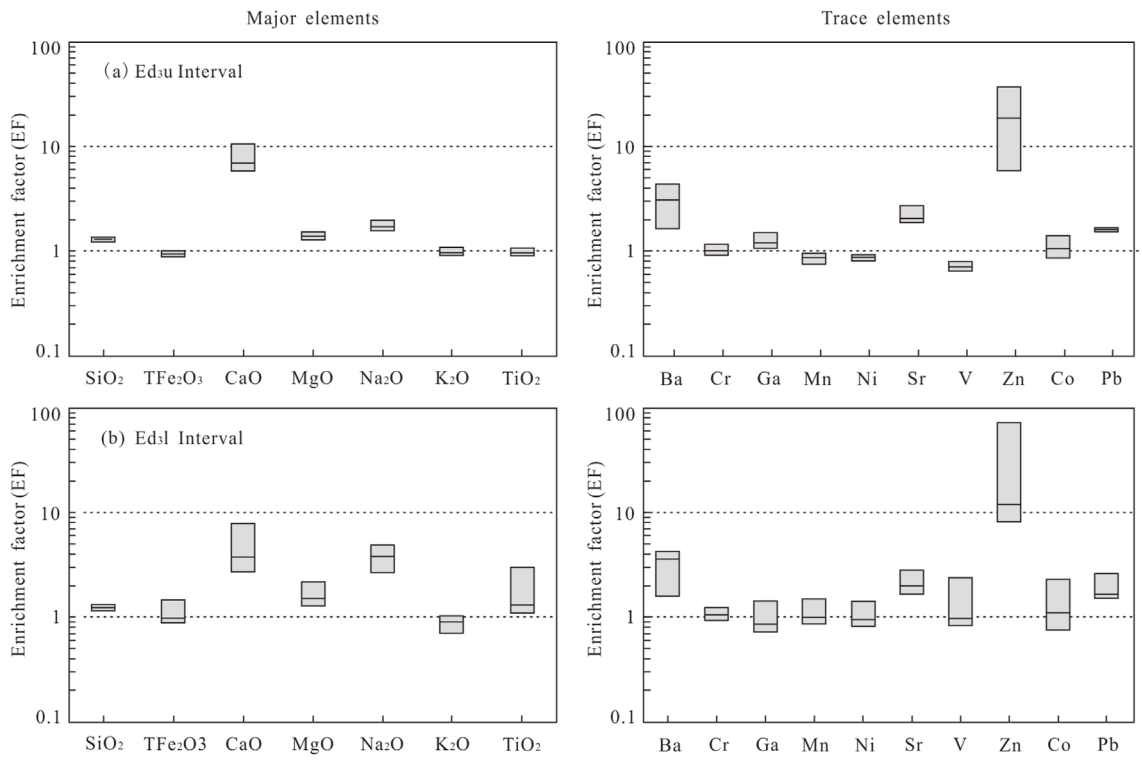

FIGURE 4
Enrichment factors of major and trace elements for the Ed_3u **(A)** and Ed_3l **(B)** intervals in the Nanpu Sag. Note: The extent of the boxes represents the range of values (min-max) and the inner line shows the mean value.

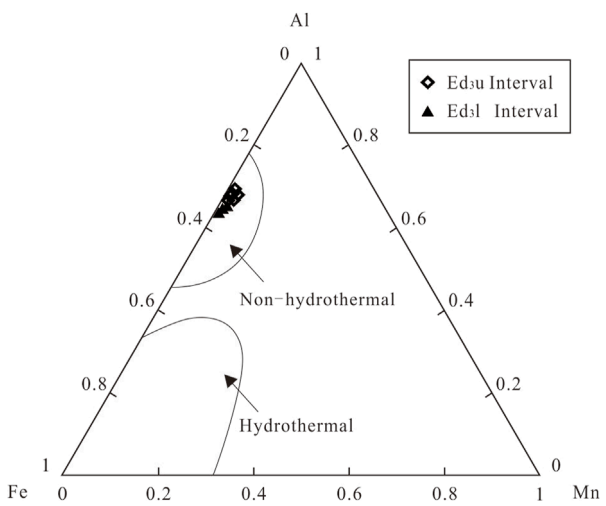

FIGURE 5
Al-Fe-Mn diagram of the Ed_3l and Ed_3u intervals in the Nanpu Sag (after Adachi et al., 1986).

source of tetrahymanol seems to be bacterivorous ciliates, which thrive at the interface between aerobic and anoxic zones in stratified water columns (Hakimi et al., 2016; Yuan et al., 2017). This compound was commonly observed in the analyzed samples. The gammacerane index, expressed as gammacerane/(gammacerane + C_{30} hopane), was less than 0.2 (Figure 7E). C_{19} and C_{20} tricyclic terpane are mainly derived from terrigenous higher plants (Adegoke et al., 2015). Higher C_{19}/C_{23} tricyclic terpene ($C_{19}/C_{23}TT$) and C_{20}/C_{23} tricyclic terpene ($C_{19}/C_{23}TT$) indicate more terrestrial organic matter input (Hao et al., 2011). These two ratios were comparable in the Ed_3l and Ed_3u intervals (Figure 7F). The former had $C_{19}/C_{23}TT$ and $C_{20}/C_{23}TT$ ranging from 0.09 to 2.07 and 0.28–1.63, respectively, and the latter from 0.05 to 1.01 and 0.17–0.80, respectively. This implies that differential terrestrial organic matter inputs were present in the Ed_3l and Ed_3u intervals.

5 Discussions

5.1 Paleoclimate

The migration and distribution of specific elements in sediments vary significantly under different climatic conditions (Moradi et al., 2016). Recently, C-value is widely employed to investigate paleoclimate changes. It is based on the hypothesis that Fe, Mn, Cr, Co, Ni, and V are typically enriched within humid conditions, whereas Ca, Mg, Ba, Sr, K, and Na are concentrated within arid conditions (Fedo et al., 1995; Li et al., 2020). The C-value is calculated as follows: C-value = ∑(Fe + Mn + Cr + Co + Ni + V)/∑(Ca + Mg + Ba + Sr + K + Na) (presented as 10^{-6}). Generally, C-value 0.6 suggests intense chemical weathering within humid climate (Qiu et al., 2015). The C-values of the Ed_3l interval ranged

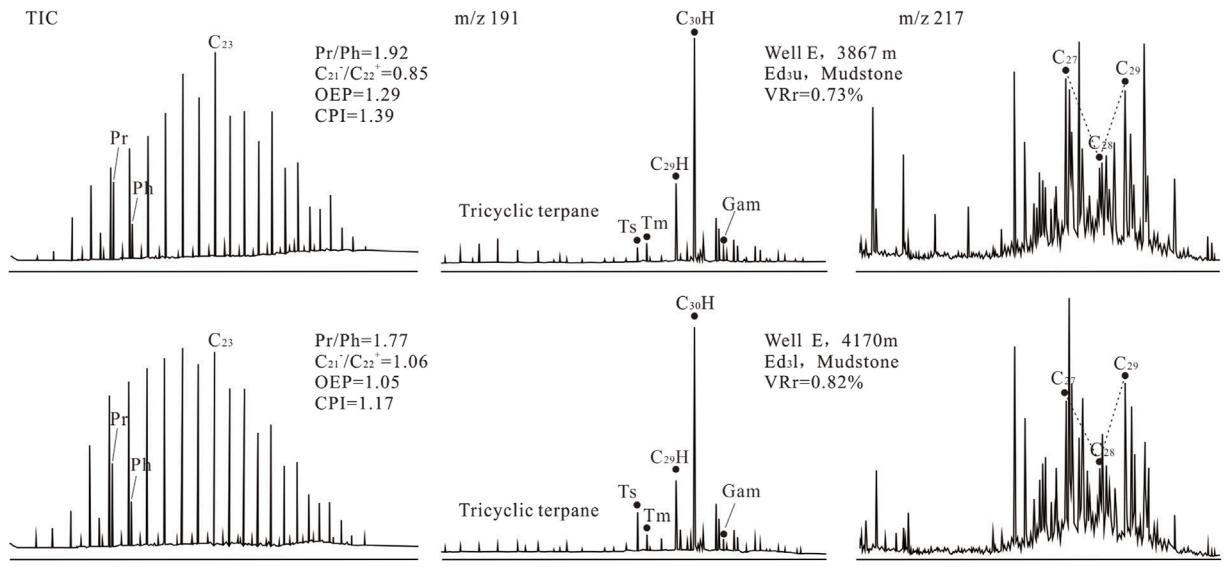

FIGURE 6
Biomarker fingerprints for the Ed_3l and Ed_3u intervals in the Nanpu Sag.

from 0.32 to 0.45, with an average of 0.40. An increasing trend from bottom to top was observed in the Ed_3l interval (Figure 8), indicating that the paleoclimate changed from semi-arid to semi-humid. The C-values of the Ed_3u interval varied between 0.30 and 0.39, with an average of 0.36. In contrast, a decreasing trend from bottom to top was observed in the Ed_3u interval (Figure 8), suggesting that the paleoclimate shifted from semi-arid to semi-humid conditions.

The content of carbonate minerals (e.g., calcite, dolomite, aragonite) in sediments is particularly sensitive to paleoclimate changes (Gyawali et al., 2019). Two origins have been proposed to explain carbonate minerals in sediments. Protogenous components are derived from the weathering and denudation of carbonate-bearing parent rocks around the lake basin. In contrast, authigenic components are those precipitated by chemical and biological sedimentation in the lake basin, which is closely linked to climate change. Dean et al. (2015) proposed that increasing content of authigenic carbonate minerals in sediments indicates the transition from humid climate to arid climate. Previous studies have shown that the provenance of Paleogene sediments in the Nanpu Sag is the granite rocks of the Yanshan fold belt, excluding carbonate rocks (Lei et al., 2021a). That is, the carbonate minerals detected in the analyzed samples are authigenic and can be used as paleoclimatic indicators. The content of carbonate minerals in the Ed_3l interval ranged from 8.3% to 17.8%, with an average of 13.3%. A decreasing trend from bottom to top indicated that the paleoclimate had changed to humid conditions. The content of carbonate minerals in the Ed_3u interval varied between 11.7% and 23.8%, with an average of 17.4%. In contrast, an increasing trend from bottom to top suggested that the paleoclimate had shifted to arid conditions. This is consistent with the paleoclimate changes inferred from the C-value (Figure 9A). Variations in paleoclimatic conditions lead to significant differences in the deposition environment by regulating factors such as weathering intensity, primary productivity, and water column conditions, etc.

5.2 Paleoenvironment

5.2.1 Paleoproductivity condition

Paleoproductivity in the water body is fueled by various unicellular planktonic organisms, which serves as the material foundation for the accumulation of organic matter in sediments (Pedersen and Calvert, 1990). Biogenic Ba involving plankton decay has been proved to be a reliable proxy for paleomarine productivity (Paytan and Griffith, 2007; Plewa et al., 2006; Tribovillard et al., 2012), specifically, concentration of 200–1,000 μg/g indicates a medium productivity and 1,000–5000 μg/g represents a high productivity. However, estimating paleolacustrine productivity with biogenic Ba is rarely reported. To avoid interference from terrigenous debris, the biogenic Ba in a sample can be estimated using the following formula: $Ba_{bio} = Ba_{total} - Al_{total} \times (Ba/Al)_{PASS}$, where Ba_{bio} represents the biogenic concentration of Ba, Ba_{total} and Al_{total} refer to the total concentrations of Ba and Al in the sediment, respectively. A value of 0.0075 is adopted as the Ba/Al ratio in the PAAS. Results show that the Ed_3l and Ed_3u intervals had high Ba_{bio} values, ranging of 800–2150μg/g and 785–2103μg/g, respectively, indicating a medium to high paleoproductivity. This is consistent with the paleoproductivity inferred from the abundance of planktonic algae fossils in sediments. Abundant planktonic algal fossils were observed in the Ed_3l and Ed_3u intervals, with content up to 16%–50% and 22%–40% (Figure 8), respectively. There was no significant correlation between TOC values and Ba_{bio} values for most samples (Figure 9B). This phenomenon suggests that, in addition to aquatic organisms, terrigenous higher plants have contributed to the accumulation of organic matter in the Ed_3l and Ed_3u intervals. This matches well with mixed organic matter inferred from the relative abundance of C_{27}, C_{28}, C_{29} regular steranes.

5.2.2 Paleowater depth condition

Investigation on modern sediments shows that certain elements, e.g., Mn and Fe, are significantly different during sedimentation. Mn

10.3389/feart.2024.1525594

TABLE 5 Biomarker parameters for the Ed_3l and Ed_3u intervals in the Nanpu Sag.

SN	Depth (m)	Interval	*n*-alkanes and isoprenoids							Terpanes (m/z = 191)						Steranes (m/z = 217)				
										Tricyclic terpanes		Hopane terpanes				Regular steranes (%)			C_{29}20S/(20R+20S)	C_{29}ββ/(αα+ββ)
			Pr/nC_{17}	Ph/nC_{18}	Pr/Ph	C_{21}^{-}/C_{22}^{+}	CPI	OEP	MP	C_{19}/C_{23}	C_{20}/C_{23}	Ts/Tm	G/(G+C_{30}	C_{29}/C_{30}	C_{29}Ts/C_{29}	C_{27}	C_{28}	C_{29}		
1	3720	Ed3u	1.74	0.34	4.41	0.79	1.27	1.28	C_{23}	0.21	0.65	0.26	0.02	0.99	0.16	0.28	0.26	0.46	0.28	0.41
2	3747	Ed3u	1.21	0.34	3.38	0.82	1.29	1.28	C_{23}	0.35	0.79	0.53	0.03	0.83	0.23	0.30	0.23	0.48	0.28	0.41
3	3760	Ed3u	1.97	0.57	3.10	0.80	1.48	1.16	C_{23}	0.05	0.17	0.25	0.02	0.64	0.24	0.28	0.21	0.51	0.31	0.41
4	3785	Ed3u	1.10	0.44	2.74	1.07	1.48	1.25	C_{23}	0.41	0.48	0.69	0.03	0.50	0.21	0.31	0.21	0.48	0.31	0.40
5	3867	Ed3u	0.98	0.43	1.92	0.85	1.39	1.29	C_{23}	0.31	0.36	0.73	0.04	0.43	0.42	0.37	0.24	0.39	0.27	0.47
6	3880	Ed3u	0.96	0.44	1.97	0.89	1.41	1.29	C_{23}	0.12	0.19	0.87	0.02	0.54	0.42	0.38	0.22	0.40	0.33	0.46
7	3920	Ed3u	0.94	0.45	2.03	0.79	1.3	1.28	C_{23}	0.32	0.30	0.71	0.05	0.46	0.27	0.33	0.22	0.46	0.32	0.47
8	3965	Ed3u	0.86	0.47	1.93	0.78	1.50	1.31	C_{23}	1.01	0.80	1.16	0.05	0.32	0.39	0.34	0.28	0.38	0.40	0.55
9	3975	Ed3u	0.76	0.44	2.16	1.09	1.45	1.35	C_{23}	0.55	0.72	1.52	0.07	0.33	0.54	0.27	0.33	0.41	0.44	0.57
10	4060	Ed3l	0.62	0.34	1.78	0.91	1.23	1.15	C_{23}	0.21	0.48	0.88	0.08	0.37	0.38	0.37	0.24	0.39	0.38	0.58
11	4070	Ed3l	0.58	0.34	1.62	0.88	1.20	1.13	C_{23}	0.90	0.66	0.74	0.12	0.45	0.44	0.38	0.22	0.40	0.40	0.59
12	4083	Ed3l	0.58	0.33	1.67	0.89	1.21	1.13	C_{23}	0.90	0.71	1.35	0.11	0.33	0.40	0.33	0.22	0.46	0.40	0.59
13	4090.2	Ed3l	0.46	0.28	1.78	0.85	1.08	1.12	C_{23}	0.61	0.64	1.21	0.11	0.36	0.37	0.35	0.29	0.36	0.41	0.52
14	4092.5	Ed3l	0.64	0.41	1.65	0.80	1.21	1.11	C_{23}	0.17	0.52	1.51	0.14	0.30	0.81	0.35	0.31	0.34	0.38	0.56
15	4100	Ed3l	0.59	0.34	1.63	0.82	1.20	1.13	C_{23}	0.59	0.53	1.04	0.08	0.35	0.50	0.44	0.25	0.31	0.38	0.54
16	4120	Ed3l	0.65	0.38	1.48	0.80	1.24	1.15	C_{23}	0.31	0.29	1.36	0.11	0.28	0.53	0.36	0.19	0.45	0.40	0.60
17	4170	Ed3l	0.66	0.33	1.77	1.06	1.17	1.05	C_{21}	0.50	0.44	2.49	0.13	0.34	0.72	0.42	0.19	0.39	0.38	0.66
18	4215.5	Ed3l	0.62	0.24	2.67	0.96	1.15	1.05	C_{21}	0.09	0.28	1.16	0.07	0.18	0.51	0.33	0.23	0.44	0.41	0.67

(Continued on the following page)

TABLE 5 (*Continued*) Biomarker parameters for the Ed_3l and Ed_3u intervals in the Nanpu Sag.

SN	Depth (m)	Interval	*n*-alkanes and isoprenoids							Terpanes (m/z = 191)						Steranes (m/z = 217)				
										Tricyclic terpanes		Hopane terpanes				Regular steranes (%)			$C_{29}20S/(20R+20S)$	$C_{29}\beta\beta/(\alpha\alpha+\beta\beta)$
			Pr/nC_{17}	Ph/nC_{18}	Pr/Ph	C_{21}^{-}/C_{22}^{+}	CPI	OEP	MP	C_{19}/C_{23}	C_{20}/C_{23}	Ts/Tm	G/(G+C_{30})	C_{29}/C_{30}	$C_{29}Ts/C_{29}$	C_{27}	C_{28}	C_{29}		
19	4216.3	Ed_3l	0.39	0.16	2.58	1.43	1.18	1.10	C_{21}	1.57	0.91	2.53	0.04	0.27	1.07	0.36	0.19	0.45	0.41	0.64
20	4218.7	Ed_3l	0.66	0.20	3.29	1.13	1.20	1.06	C_{21}	1.53	1.47	4.18	0.05	0.24	1.22	0.33	0.21	0.46	0.40	0.64
21	4219.5	Ed_3l	0.52	0.16	3.02	0.87	1.23	1.03	C_{21}	2.07	1.63	0.39	0.02	0.16	1.49	0.40	0.20	0.40	0.36	0.57

Note: CPI, Carbon Preference Index (2 $[C_{23}+C_{25}+C_{27}+C_{29}]/[C_{22}+2(C_{24}+C_{26}+C_{28}+C_{30})]$); OEP, Odd-Even Predominance ($[C_{25}+C_{27}+C_{29}]/2\ [C_{26}+C_{28}]$); MP, Max Peak.; G/(G+$C_{30}$), Gammacerane/(Gammacerane+C_{30} hopane); C_{29}/C_{30}, C_{29} norhopane/C_{30} hopane; $C_{29}Ts/C_{29}$, C_{29} norneohopane/C_{30} hopane.

has strong stability and tends to be enriched in deep water after long-distance migration (Toyoda, 1993). In contrast, Fe is unstable and enriched in shallow water after short-distance migration. Therefore, the Mn/Fe ratios are commonly employed to investigate paleowater depth. A high value indicates the presence of a deep-water environment and *vice versa*. Results show that the Mn/Fe ratios of the Ed_3l interval ranged from 136.6×10^{-4} to 160.8×10^{-4}, with an average of 148.9×10^{-4}. An increasing trend from bottom to top was observed in the Ed_3l interval (Figure 8), indicating that the paleowater depth changed from shallow water to deep water. The Mn/Fe ratios of the Ed_3u interval varied between 133.4×10^{-4}–149.5×10^{-4}, with an average of 144.1×10^{-4}. In contrast, a decreasing trend from bottom to top was observed in the Ed_3u interval, suggesting that the paleowater depth evolved from deep water to shallow water. Note that in Figure 8, the Mn/Fe values exhibit similar trends as C-values in the vertical. This phenomenon suggests that the variation in water depth during the Ed_3 period was controlled by climatic factors. Enhanced lake evaporation and weakened atmospheric precipitation occur in the transition from humid to arid climate, resulting in the transformation of lakes from deep-water to shallow-water environment, and *vice versa*.

The fluctuation in water depth during the Ed_3 period caused the different burial efficiency of organic matter (Figure 9C). Generally, a reduction condition with stable water stratification commonly developed in a deep-water environment, whereas an oxidation condition with unstable water stratification formed in a shallow-water environment (Lei et al., 2021b). Hence,the burial efficiency of organic matter in the deep-water environment is significantly higher than that in the shallow-water environment.

5.2.3 Paleosalinity condition

Trace elements such as Sr and Ba are particularly sensitive to changes in water salinity. These two elements commonly occur as the form of ions in low salinity water. Sr has stronger migration ability than Ba in water body. Increasing water salinity can cause Ba^{2+} precipitating as $BaSO_4$ prior to Sr^{2+} precipitating as $SrSO_4$, resulting in a higher concentration of Sr in sediments compared to Ba. As a result, the Sr concentration and Sr/Ba ratio recorded in sediments is positively correlated with the paleosalinity. In general, the Sr concentration (presented as 10^{-6}) less than 300 was a fresh water environment, 300–800 was a brackish water environment, 800–1,000 was a saline water environment, and more than 1,000 was an ultra-saline water environment. Wei and Algeo (2019) held that Sr/Ba <0.2 was fresh water, 0.2–0.5 was brackish water, and >0.5 was saline water. Sr concentrations in the Ed_3l and Ed_3u intervals were in a range of 257.90–405.20 (average 313.30) and 273.10–361.50 (average 296.90), respectively, with corresponding Sr/Ba ratios were 0.14–0.32 (average 0.20) and 0.15–0.29 (average 0.22), respectively. These indicators suggest that the water body fluctuated between fresh and brackish water (Figure 9D). Note that in Figure 8, The Sr/Ba values and C-values have a rough mirroring relationship in the vertical. This phenomenon implies that the changes of water salinity during the Ed_3 period was also controlled by climatic factors. When the humid climate changes to arid climate, the concentration of various ions in the water tends to concentrate due to the combination of enhanced lake evaporation and weakened atmospheric precipitation, and *vice versa*.

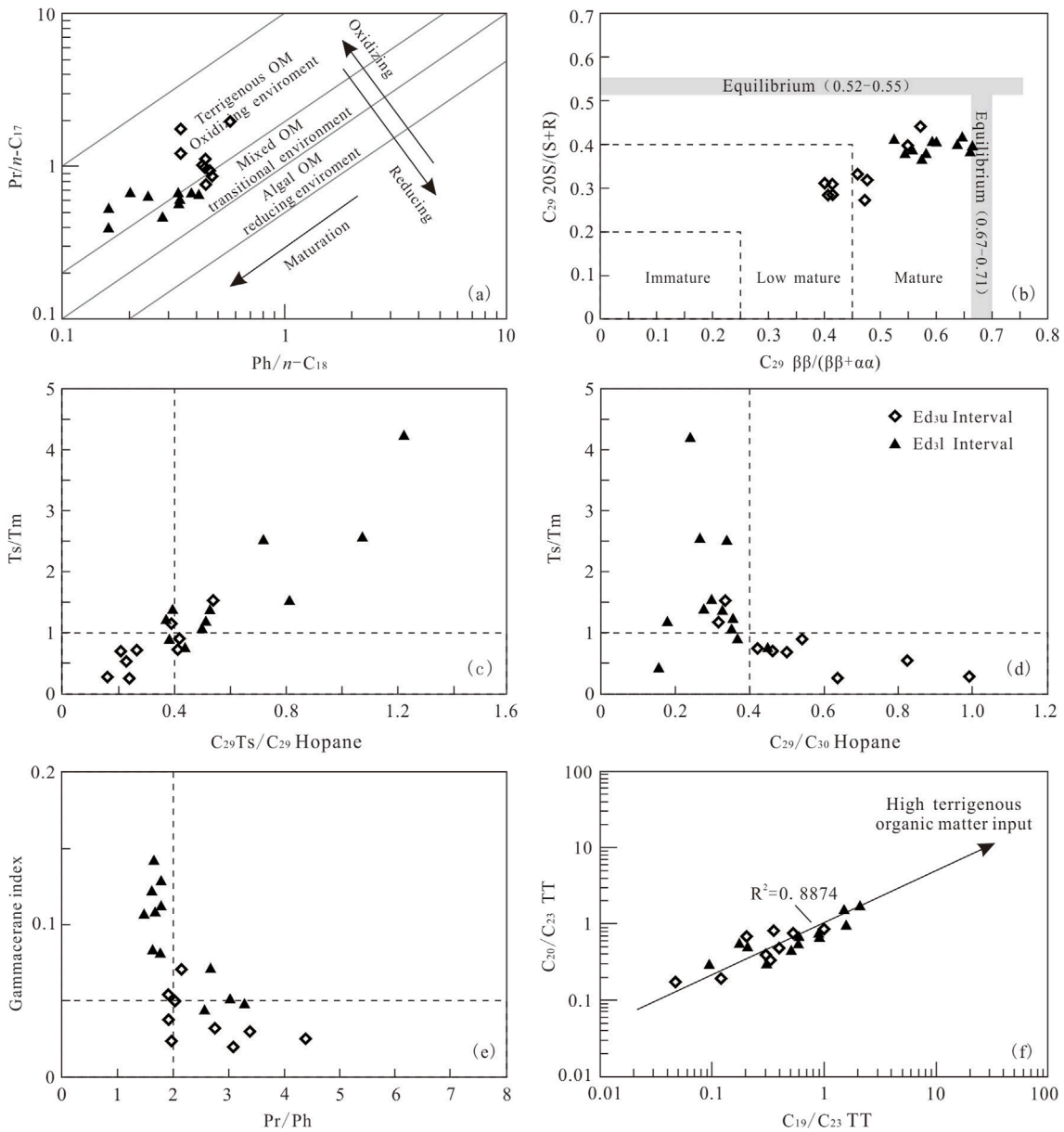

FIGURE 7
Cross-plots of various biomarker parameters **(A–F)** for the Ed_3l and Ed_3u intervals in the Nanpu Sag.

Abundant gammacerane is a sign of stratification in high salinity water (Ten Haven et al., 1989). Gammacerane index less than 0.2 for a freshwater environment, and more than 0.2 for a saltwater environment (Yuan et al., 2017). The gammacerane indexes of the Ed_3l and Ed_3u intervals were 0.04–0.14 and 0.02–0.07, respectively, with an average value of 0.09 and 0.04, respectively, indicating that fresh and brackish water coexisted during this period.

In summary, the suitable salinity during the Ed_3 period was conducive to the flourishing of aquatic organisms. This can be evidenced by abundant planktonic algal fossils, e.g., Chlorella Gracilis, Granulosus, Reticulosus, Rugosus, Spinococcus, Ceratophyllum, etc., provided by the PetroChina Jidong Oilfield Company.

5.2.4 Paleoredox condition

Redox-sensitive trace elements such as V and Ni can be differentiated under different redox conditions. These two elements are prone to precipitate at anoxic water column and dissolve at oxic water column, and not affected by the diagenesis (Scheffler et al., 2006; Tribovillard et al., 2006). Most samples have no obvious enrichment or depletion in the both V and Ni elements, with the EFs of 0.66–2.36 and 0.82–1.39, respectively (Figure 4). This phenomenon is a response to the weak reduction-weak oxidation conditions. Generally, V/(V + Ni) < 0.46 was an oxic condition with weak stratification, 0.60–0.84 was a dysoxic condition with medium stratification, and >0.84 was an anoxic condition with intense stratification and H_2S in the bottom water (Hatch and

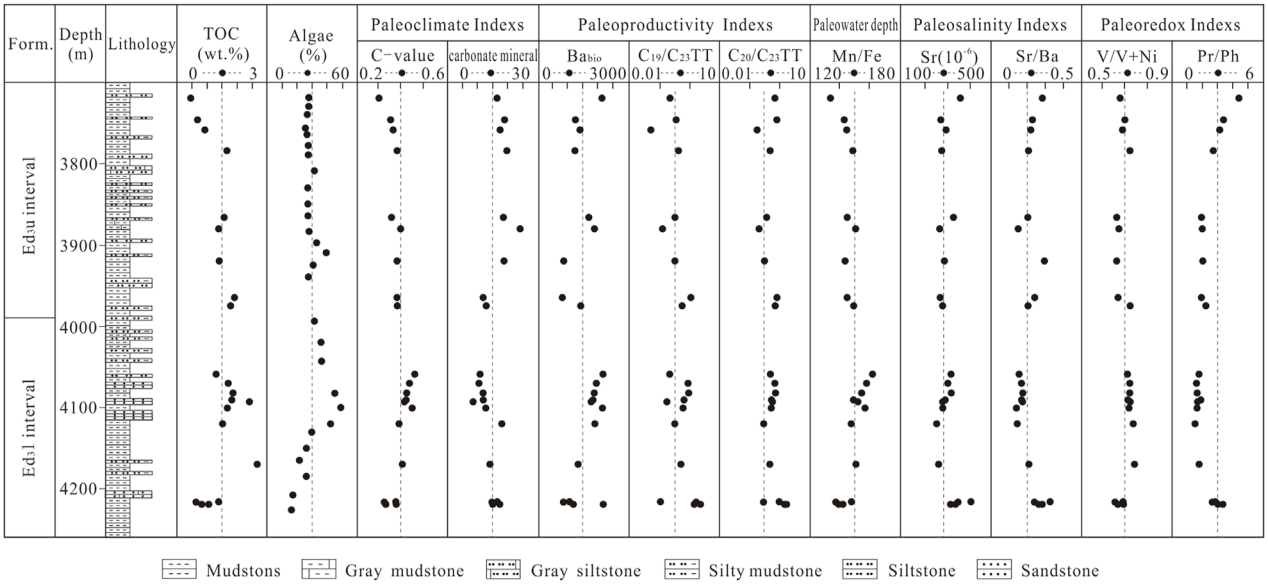

FIGURE 8
Vertical distribution of palaeoclimate and palaeoenvironment indexes for the Ed_3l and Ed_3u intervals in Well E. Note: Algal fossil data were collected from the PetroChina Jidong Oilfield Company.

Leventhal, 1992). The Ed_3l and Ed_3u intervals had a narrow variation in the V/(V + Ni) ratios, ranging from 0.65 to 0.73 (averaging 0.70) and 0.65 to 0.71 (averaging 0.68), respectively. It suggests that the activity of water body during the deposition of the Ed_3l and Ed_3u intervals was weak, with a predominantly weak reduction-weak oxidation condition. This is consistent with the sedimentary structures observed in the mudstone core, where the alternating micro-layered, layered, and massive structures appear to be a response to the weak reducing-weak oxidizing condition.

The Pr/Ph ratio is also an important parameter to characterize redox conditions. Previous reported that Pr/Ph < 1 represented anoxic conditions, 1.0–3.0 suggested slightly oxic conditions, and >3 indicated oxic conditions (Peters et al., 2005a). The Pr/Ph ratio may be influenced by maturation. The influence of maturation on the Pr/Ph ratios could be ignored because all the samples were of low maturity. The Pr/Ph ratios of the Ed_3l and Ed_3u intervals were 1.48–3.29 and 1.92–4.41, respectively, with an average value of 2.07 and 2.62, respectively, which further indicated that the water body was dominated by weak reduction-weak oxidation environment. As shown in Figure 7A, the discriminant diagram of Pr/nC_{17} and Ph/nC_{18} also support this conclusion.

Organic matter accumulation in the Ed_3 member was clearly controlled by redox conditions. It can be inferred from the positive correlation of TOC values with V/(V + Ni) ratios (Figure 9E) and negative correlation with Pr/Ph ratios (Figure 9F) in most samples. A few samples deviated from the trend line, which may be related to abundant terrigenous organic matter with the degradation-resisting structure.

5.3 Development model for organic-matter accumulation in fine-grained sediments

Previous studies suggested that organic matter accumulation in fine-grained sediments is influenced by multiple elements in the paleolacustrine environment, which is controlled by the co-evolution of tectonic and climatic conditions. The Nanpu Sag underwent rapid subsidence during the Ed_3 period, with a maximum subsidence rate of 550 m/Ma (Wang et al., 2012). On the one hand, rapid subsidence provided sufficient accommodation space particularly in the deposition centers of the Linque sub-sag and Caofeidian sub-sag, with a maximum deposition thickness of up to 900 m. On the other hand, a semi-deep/deep lake environment occurred during the Ed_3 period, benefiting from subsidence rates that exceeded material supply rates. The paleoclimate changed between semi-humid and semi-arid conditions during the Ed_3 period. Hence, two development models of the Ed_3 source rock under semi-humid to humid and semi-arid to arid climate were established.

Owing to the combination of weakened lake evaporation and enhanced atmospheric precipitation, the existing deep-water environment was prone to forming a weak reduction condition with stable water column stratification under the semi-humid to humid climate (Figure 10A), such as in samples number 12–16. High water inflow under the semi-humid to humid climate brought considerable plant debris and terrigenous debris into the lake basin, as evidenced by moderate $C_{19}/C_{23}TT$, $C_{20}/C_{23}TT$, and Al_2O_3 ratios (Tables 3, 5). Terrigenous debris can provide abundant nutriment to support the growth of planktonic organisms, improving primary productivity. This interpretation is supported by the presence of abundant planktonic algal fossils, e.g., Chlorella Gracilis,

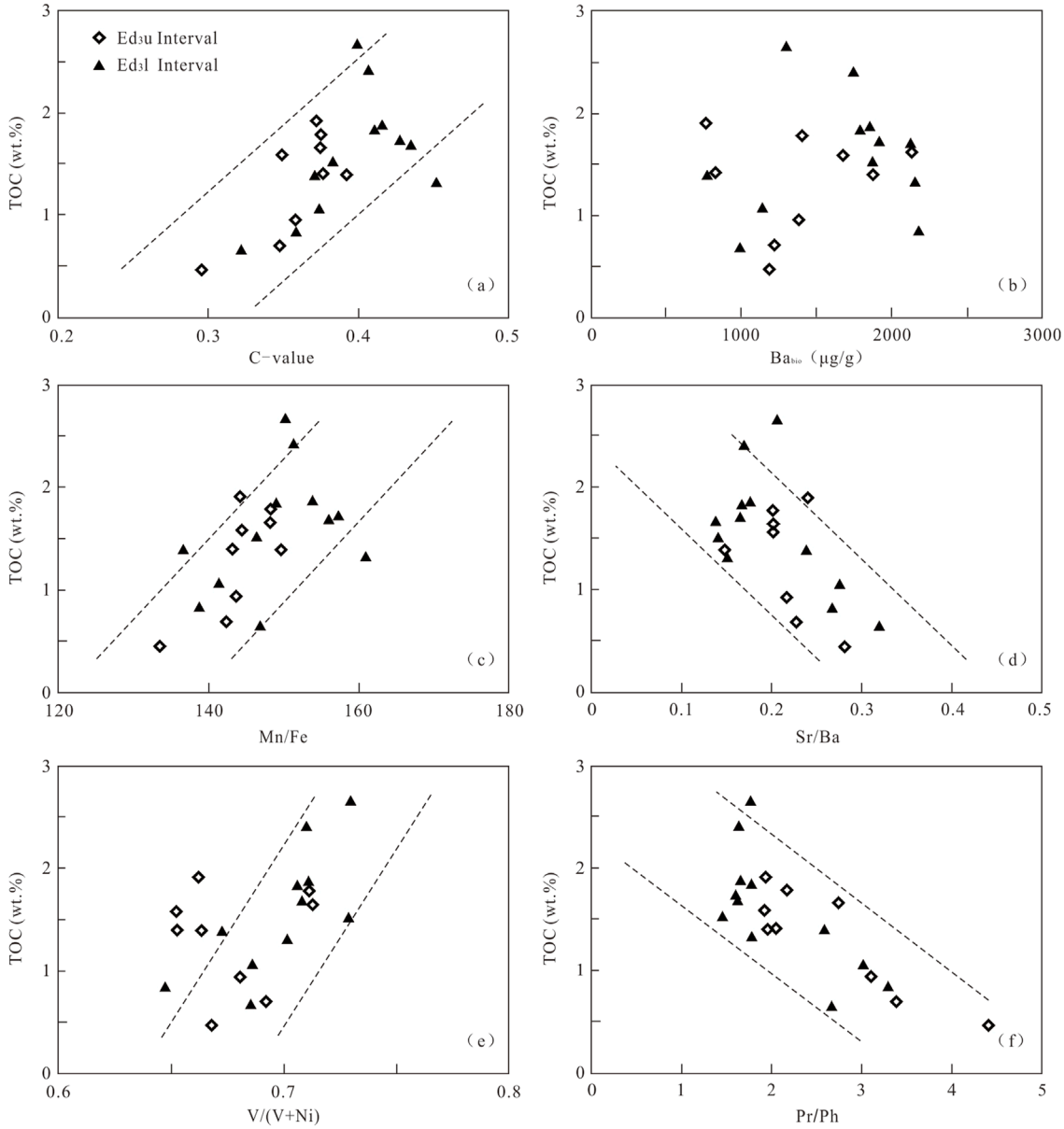

FIGURE 9
Relationship between TOC and palaeoclimate and palaeoenvironment indexes **(A–F)** for the Ed_3l and Ed_3u intervals in the Nanpu Sag.

Granulosus, Reticulosus, Rugosus, Spinococcus, Ceratophyllum Chlorellas, and Pediastrums, observed in organic-matter-rich mudstone. The accumulation of mixed aquatic and terrigenous organic matter provided material for Type II kerogen. The semi-deep to deep lake had a water temperature gradient, giving rise to stable water column stratification under gravity (represented by moderate gammacerane indexes). No commutation between the surface and bottom water at the stratification interface, resulting in a weak reduction condition (represented by high V/(V + Ni) and low Pr/Ph values). Limited degradation occurred in the aquatic and terrigenous organic matter that could be effectively preserved during burial. The coexistence of mixed organic matter input and relative reduction condition gave rise to high organic matter accumulation. Vertically, the unconventional shale oil discovered in the Ed_3 member of the Nanpu Sag corresponds to the same location as the samples number 12–16 in well E.

On the other hand, owing to the combination of enhanced lake evaporation and weakened atmospheric precipitation, the existing shallow-water environment is prone to forming a weak oxidation condition with unstable water column stratification under the semi-arid to arid climate (Figure 10B), such as samples number 1–3. The unstable water column stratification can be evidenced by low gammacerane indexes. Low water inflow under the semi-arid to arid climate brought limited plant debris and terrigenous debris into the lake basin, as evidenced by low $C_{19}/C_{23}TT$, $C_{20}/C_{23}TT$, and Al_2O_3 ratios. As a result, insufficient nutriment presentin these terrigenous debris could only support medium primary productivity. As oxygen-sensitive material, hydrogen-rich organic

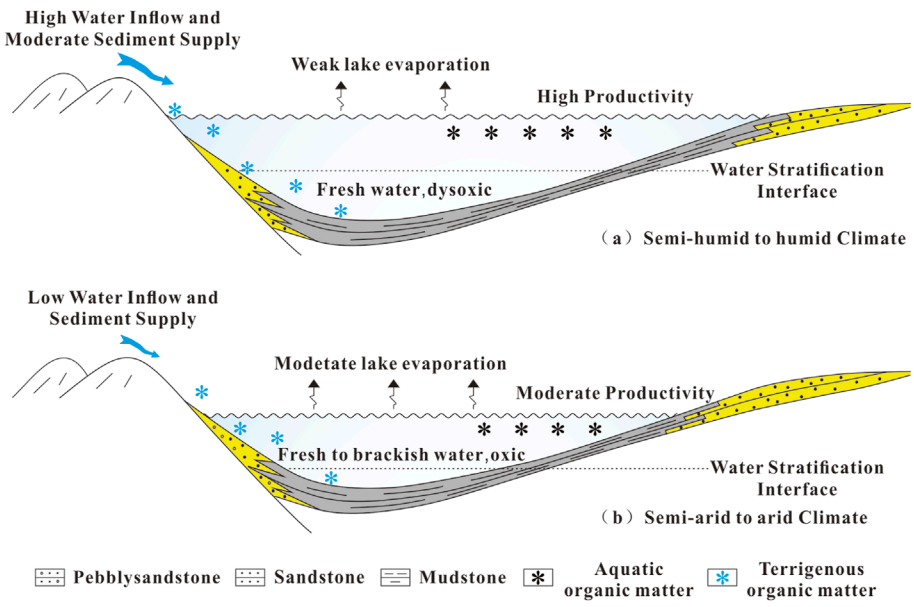

FIGURE 10
Development model **(A, B)** of source rock for the Ed_3l and Ed_3u intervals in the Nanpu Sag.

matter might be preferentially oxidized and subsequently degraded under an aerobic condition. This is supported by the observation of a positive correlation between TOC and V/(V + Ni) values, as well as a negative correlation between TOC and Pr/Ph values. The coexistence of limited organic matter input and relative oxidation conditions resulted in low organic matter accumulation. The exploration potential of unconventional shale oil in this location has not yet been realized.

6 Conclusion

Based on mineralogical and geochemical analysis of forty-nine mudstone samples, following conclusions can be obtained:

(1) Fine-grained sediments record abundant information of paleoclimate and paleoenvironment in geological history. The integrated mineralogy and geochemistry are a valid method in understanding the paleoclimate and paleoenvironment.
(2) The Ed_3 source rocks exhibit strong heterogeneity, especially in terms of organic matter abundance, type, and hydrocarbon-generation potential. Overall, they are dominated by general-quality to high-quality source rocks with mixed kerogen at low mature to mature stage.
(3) The alternated paleoclimate between semi-humid to semi-arid during the Ed_3 period governed the fluctuations of paleoenvironment elements. Two development models of the Ed_3 source rock under semi-humid to humid and semi-arid to arid climate were established to interpret the deposition process involving organic matter supply and preservation/degradation.
(4) The exploration of unconventional shale oil in the Ed_3 member of Nanpu Sag should focus on the organic-matter-rich mudstones developed in the humid climate. Reconstruction of the development model of organic-matter-rich mudstone based on the paleoenvironment controlled by the co-evolution of tectonic and climatic factors is a valid method for understanding unconventional shale oil exploration potential.

Data availability statement

The original contributions presented in the study are included in the article/supplementary material, further inquiries can be directed to the corresponding authors.

Author contributions

SY: Writing–review and editing, Conceptualization, Data curation, Investigation, Writing–original draft, Methodology, Formal Analysis, Project administration, Visualization. AY: Data curation, Methodology, Supervision, Formal Analysis, Project administration, Validation, Writing–review and editing. JC: Methodology, Supervision, Conceptualization, Validation, Investigation, Writing–review and editing. CL: Conceptualization, Investigation, Methodology, Writing–review and editing, Funding acquisition, Resources, Supervision, Validation. ZW: Data curation, Formal Analysis, Investigation, Software, Writing–review and editing. ZZ: Formal Analysis, Supervision, Validation, Writing–review and editing. YZ: Data curation, Methodology, Software, Writing–review and editing. YW: Data curation, Methodology, Software, Writing–review and editing. XH: Data curation, Methodology, Software, Writing–review and editing. ZM: Data curation, Methodology, Software, Writing–review and editing.

Funding

The author(s) declare that financial support was received for the research, authorship, and/or publication of this article. This study was financially supported by the National Natural Science Foundation of China (Nos. 72474067), the Science and Technology Planning Project of Tangshan City, China (Nos. 22130213H), and the Liaoning Key Laboratory of Green Development of Mineral Resources, China (Nos. LNTU/GDMR-2316).

Acknowledgments

We thank the PetroChina Jidong Oilfield Company for kindly providing subsurface datasets in this study.

Conflict of interest

Author AY was employed by No. 6 Oil Production Plant of Daqing Oilfield Co. Ltd.

The remaining authors declare that the research was conducted in the absence of any commercial or financial relationships that could be construed as a potential conflict of interest.

Generative AI statement

The author(s) declare that no Generative AI was used in the creation of this manuscript.

Publisher's note

All claims expressed in this article are solely those of the authors and do not necessarily represent those of their affiliated organizations, or those of the publisher, the editors and the reviewers. Any product that may be evaluated in this article, or claim that may be made by its manufacturer, is not guaranteed or endorsed by the publisher.

References

Adachi, M., Yamamoto, K., and Sugisaki, R. (1986). Hydrothermal chert and associated siliceous rocks from the northern Pacific their geological significance as indication od ocean ridge activity. *Sediment. Geol.* 47, 125–148. doi:10.1016/0037-0738(86)90075-8

Adegoke, A. K., Adegoke, W. H., Hakimi, M. H., and Sarki Yandoka, B. M. (2015). Geochemical characterisation and organic matter enrichment of upper cretaceous gongila shales from Chad (bornu) basin, northeastern Nigeria: bioproductivity versus anoxia conditions. *J. Petroleum Sci. Eng.* 135, 73–87. doi:10.1016/j.petrol.2015.08.012

Algeo, T. J., and Tribovilard, N. (2009). Environmental analysis of paleo-ceanographic systems based on molybdenum-uranium covariation. *Chem. Geol.* 268, 211–225. doi:10.1016/j.chemgeo.2009.09.001

Bechtel, A., Jia, J. L., Strobl, S. A. I., Sachsenhofer, R. F., Liu, Z., Gratzer, R., et al. (2012). Palaeoenvironmental conditions during deposition of the upper Cretaceous oil shale sequences in the Songliao Basin (NE China): implications from geochemical analysis. *Org. Geochem.* 46, 76–95. doi:10.1016/j.orggeochem.2012.02.003

Cai, Q. S., Hu, M. Y., Zhang, B. M., Ngia, N., Liu, A., Liao, R. Q., et al. (2022). Source of silica and its implications for organic matter enrichment in the Upper Ordovician-Lower Silurian black shale in western Hubei Province, China: insights from geochemical and petrological analysis. *Petroleum Sci.* 19, 74–90. doi:10.1016/j.petsci.2021.10.012

Carroll, A. R., and Bohacs, K. M. (1999). Stratigraphic classification of ancient lakes: balancing tectonic and climatic controls. *Geology* 27 (2), 99–102. doi:10.1130/0091-7613(1999)027<0099:scoalb>2.3.co;2

Carroll, A. R., and Bohacs, K. M. (2001). Lake-type controls on petroleum source rock potential in nonmarine basins. *AAPG Bull.* 85 (6), 1033–1053. doi:10.1306/8626ca5f-173b-11d7-8645000102c1865d

Dai, S. F., Seredin, V. V., Ward, C. R., Hower, J. C., Xing, Y., Zhang, W., et al. (2015). Enrichment of U-Se-Mo-Re-V in coals preserved within marine carbonate successions: geochemical and mineralogical data from the Late Permian Guiding Coalfield, Guizhou, China. *Miner. Deposita* 50 (2), 159–186. doi:10.1007/s00126-014-0528-1

Dean, J. R., Jones, M. D., Leng, M. J., Noble, S. R., Metcalfe, S. E., Sloane, H. J., et al. (2015). Eastern Mediterranean hydroclimate over the late glacial and Holocene, reconstructed from the sediments of Nar lake, central Turkey, using stable isotopes and carbonate Mineralogy. *Quat. Sci. Rev.* 124, 162–174. doi:10.1016/j.quascirev.2015.07.023

Farhaduzzaman, M., Abdullah, W. H., and Islam, M. A. (2012). Depositional environment and hydrocarbon source potential of the permian gondwana coals from the barapukuria basin, northwest Bangladesh. *Int. J. Coal Geol.* 90-91, 162–179. doi:10.1016/j.coal.2011.12.006

Fedo, C. M., Nesbitt, H. W., and Young, G. M. (1995). Unraveling the effects of potassium metasomatism in sedimentary rocks and paleosols, with implications for paleoweathering conditions and provenance. *Geology* 23 (10), 921–924. doi:10.1130/0091-7613(1995)023<0921:UTEOPM>2.3.CO;2

Fu, C., Li, S. L., Li, S. L., Xu, J., and Huang, Y. (2022). Genetic types of mudstone in a closed-lacustrine to open-marine transition and their organic matter accumulation patterns: a case study of the paleocene source rocks in the east China sea basin. *J. Petroleum Sci. Eng.* 208, 109343. doi:10.1016/j.petrol.2021.109343

Garzanti, E., Andò, S., Padoan, M., Vezzoli, G., and El Kammar, A. (2015). The modern Nile sediment system: processes and products. *Quat. Sci. Rev.* 130, 9–56. doi:10.1016/j.quascirev.2015.07.011

Ghassal, B. I., Littke, R., Atfy, H. E., Sindern, S., Scholtysik, G., El Beialy, S., et al. (2018). Source rock potential and depositional environment of Upper Cretaceous sedimentary rocks, Abu Gharadig Basin, Western Desert, Egypt: an integrated palynological, organic and inorganic geochemical study. *Int. J. Coal Geol.* 186, 14–40. doi:10.1016/j.coal.2017.11.018

Gyawali, A. R., Wang, J. B., Ma, Q. F., Wang, Y., Xu, T., Guo, Y., et al. (2019). Paleo-environmental change since the Late Glacial inferred from lacustrine sediment in Selin Co, central Tibet. *Palaeogeogr. Palaeoclimatol. Palaeocology* 516, 101–112. doi:10.1016/j.palaeo.2018.11.033

Hakimi, M. H., Abdullah, W. H., Alqudah, M., Makeen, Y. M., and Mustapha, K. A. (2016). Organic geochemical and petrographic characteristics of the oil shales in the Lajjun area, Central Jordan: origin of organic matter input and preservation conditions. *Fuel* 181, 34–45. doi:10.1016/j.fuel.2016.04.070

Hanson, A. D., Zhang, S. C., Moldowan, J. M., Liang, D. G., and Zhang, B. M. (2000). Molecular organic geochemistry of the tarim basin, northwest China. *AAPG Bull.* 84, 1109–1128. doi:10.1306/A9673C52-1738-11D7-8645000102C1865D

Hao, F., Zhou, X. H., Zhu, Y. M., and Yang, Y. Y. (2011). Lacustrine source rock deposition in response to co-evolution of environments and organisms controlled by tectonic subsidence and climate, Bohai Bay Basin, China. *Org. Geochem.* 42, 323–339. doi:10.1016/j.orggeochem.2011.01.010

Hatch, J. R., and Leventhal, J. S. (1992). Relationship between inferred redox potential of the depositional environment and geochemistry of the Upper Pennsylvanian (Missourian) Stark Shale Member of the Dennis Limestone, Wabaunsee County, Kansas, U.S.A. *Chem. Geol.* 99, 65–82. doi:10.1016/0009-2541(92)90031-Y

Jiang, F. J., Guo, J., and Pang, X. Q. (2023). Joint evaluation of three types of oil-gas resources in whole petroleum system of Nanpu sag, Bohai Bay Basin. *Acta Pet. Sin.* 44 (9), 1472–1486. doi:10.7623/syxb202309006

Johnston, M. N., Eble, C. F., O'Keefe, J. M. K., Freeman, R. L., and Hower, J. C. (2017). Petrology and palynology of the Middle Pennsylvanian Leatherwood coal bed, Eastern Kentucky: Indications for depositional environments. *Int. J. Coal Geol.* 181, 23–38. doi:10.1016/j.coal.2017.08.008

Kaufman, A. J., and Knoll, A. H. (1995). Neoproterozoic variations in the C-isotopic composition of seawater: stratigraphic and biogeochemical implications. *Precambrian Res.* 73, 27–49. doi:10.1016/0301-9268(94)00070-8

Lei, C., Yin, S. Y., Shi, S. B., and Meng, L. (2021a). Depositional environment and sediment provenance of the third member of the Palaeogene Shahejie Formation in the

Nanpu Sag of the Bohai Bay Basin, eastern China: Evidence from trace and rare earth element geochemistry. *Geol. J.* 56 (11), 5780–5791. doi:10.1002/gj.4272

Lei, C., Yin, S. Y., Ye, J. R., Wu, J., Wang, Z., and Gao, B. (2021b). Characteristics and deposition models of the Paleocene source rocks in the Lishui Sag, East China Sea Shelf Basin: Evidences from organic and inorganic geochemistry. *J. Petroleum Sci. Eng.* 200, 108342. doi:10.1016/j.petrol.2021.108342

Li, Q., Wu, S., Xia, D., You, X., Zhang, H., and Lu, H. (2020). Major and trace element geochemistry of the lacustrine organic-rich shales from the Upper Triassic Chang 7 Member in the southwestern Ordos Basin, China: implications for paleoenvironment and organic matter accumulation. *Mar. Petroleum Geol.* 111, 852–867. doi:10.1016/j.marpetgeo.2019.09.003

Moradi, A. V., Sarı, A., and Akkaya, P. (2016). Geochemistry of the Miocene oil shale (Hancili Formation) in the Cankiri-Corum Basin, Central Turkey: implications for Paleoclimate conditions, source–area weathering, provenance and tectonic setting. *Sediment. Geol.* 341, 289–303. doi:10.1016/j.sedgeo.2016.05.002

Morford, J. L., Emerson, S. R., Breckel, E. J., and Kim, S. H. (2005). Diagenesis of oxyanions (V, U, Re, and Mo) in pore waters and sediments from a continental margin. *Geochimica Cosmochimica Acta* 69, 5021–5032. doi:10.1016/j.gca.2005.05.015

Ocubalidet, S. G., Rimmer, S. M., and Conder, J. A. (2018). Redox conditions associated with organic carbon accumulation in the Late Devonian New Albany Shale, West-Central Kentucky, Illinois Basin. *Int. J. Coal Geol.* 190, 42–55. doi:10.1016/j.coal.2017.11.017

Paytan, A., and Griffith, E. M. (2007). Marine barite: recorder of variations in ocean export productivity. *Deep-Sea Res. Part II* 54 (5-7), 687–705. doi:10.1016/j.dsr2.2007.01.007

Pedersen, T. F., and Calvert, S. E. (1990). Anoxia vs. productivity: what controls the formation of organic–carbon–rich sediments and sedimentary Rocks? *AAPG Bull.* 74 (4), 454–466. doi:10.1306/0C9B232B-1710-11D7-8645000102C1865D

Peters, K. E., and Moldowan, J. M. (1991). Effects of source, thermal maturity, and biodegradation on the distribution and isomerization of homohopanes in petroleum. *Org. Geochem.* 17, 47–61. doi:10.1016/0146-6380(91)90039-M

Peters, K. E., Walters, C. C., and Moldowan, J. M. (2005a). *The biomarker guide volume 1: biomarkers and isotopes in the environment and human history*. New York: Cambridge University Press.

Peters, K. E., Walters, C. C., and Moldowan, J. M. (2005b). *The biomarker guide*. 2nd ed. Cambridge: Cambridge University Press.

Plewa, K., Meggers, H., and Kasten, S. (2006). Barium in sediments off northwest Africa: A tracer for paleoproductivity or meltwater events? *Paleoceanography* 21, PA2015. doi:10.1029/2005PA001136

Qiu, X. W., Liu, C. Y., Wang, F. F., Deng, Y., and Mao, G. (2015). Trace and rare earth element geochemistry of the upper Triassic mudstones in the southern Ordos basin, central China. *Geol. J.* 50 (4), 399–413. doi:10.1002/gj.2542

Quan, Y. B., Hao, F., Liu, J. Z., Zhao, D., Tian, J., and Wang, Z. (2017). Source rock deposition controlled by tectonic subsidence and climate in the western Pearl River Mouth Basin, China: Evidence from organic and inorganic geochemistry. *Mar. Petroleum Geol.* 79, 1–17. doi:10.1016/j.marpetgeo.2016.10.028

Sachsenhofer, R. F., Popov, S. V., Akhmetiev, M. A., Bechtel, A., Gratzer, R., Groβ, D., et al. (2017). The type section of the Maikop Group (Oligocene-Lower Miocene) at the Belaya River (North Caucasus): depositional environment and hydrocarbon potential. *Bulletin* 101 (3), 289–319. doi:10.1306/08051616027

Scheffler, K., Buehmann, D., and Schwark, L. (2006). Analysis of Late Palaeozoic glacial to postglacial sedimentary successions in South Africa by geochemical proxies-Response to climate evolution and sedimentary environment. *Palaeogeogr. Palaeoclimatol. Palaeoecol.* 240 (1/2), 184–203. doi:10.1016/j.palaeo.2006.03.059

Tang, L., Song, Y., Pang, X., Jiang, Z., Guo, Y., Zhang, H., et al. (2020). Effects of paleo sedimentary environment in saline lacustrine basin on organic matter accumulation and preservation: a case study from the Dongpu Depression, Bohai Bay Basin, China. *J. Petroleum Sci. Eng.* 185, 106669. doi:10.1016/j.petrol.2019.106669

Taylor, S. R., and McLennan, S. M. (1985). "The Continental Crust: its Composition and Evolution," in *An examination of the geochemical record preserved in sedimentary rocks*. Oxford London: Blackwell Scientific Publication.

Ten Haven, H. L., Rohmer, M., Rullkötter, J., and Bisseret, P. (1989). Tetrahymanol, the most likely precursor of gammacerane, occurs ubiquitously in marine sediments. *Geochimica Cosmochimica Acta* 53, 3073–3079. doi:10.1016/0016-7037(89)90186-5

Toyoda, K. (1993). Geochemical history of ancient Lake Biwa in Japan—chemical indicators of sedimentary paleo-environments in a drilled core. *Palaeogeogr. Palaeoclimatol. Palaeoecol.* 101 (1/2), 169–184. doi:10.1016/0031-0182(93)90158-F

Tribovillard, N., Algeo, T., Baudin, F., and Riboulleau, A. (2012). Analysis of marine environmental conditions based on molybdenum-uranium covariation applications to Mesozoic paleoceanography. *Chem. Geol.* 324/325, 46–58. doi:10.1016/j.chemgeo.2011.09.009

Tribovillard, N., Algeo, T. J., Lyons, T., and Riboulleau, A. (2006). Trace metals as paleoredox and paleoproductivity proxies: an update. *Chem. Geol.* 232, 12–32. doi:10.1016/j.chemgeo.2006.02.012

Tribovillard, N., Bout-Roumazeilles, V., Algeo, T., Lyons, T. W., Sionneau, T., Montero-Serrano, J. C., et al. (2008). Paleodepositional conditions in the Orca Basin as inferred from organic matter and trace metal contents. *Mar. Geol.* 254, 62–72. doi:10.1016/j.margeo.2008.04.016

Tripathy, G. R., Singh, S. K., and Ramaswamy, V. (2014). Major and trace element geochemistry of Bay of Bengal sediments: Implications to provenances and their controlling factors. *Palaeogeogr. Palaeoclimatol. Palaeoecol.* 397, 20–30. doi:10.1016/j.palaeo.2013.04.012

Volkman, J. K., Kearney, P., and Jeffrey, S. W. (1990). A new source of 4-methyl sterols and 5α(H)-stanols in sediments: Prymnesiophyte microalgae of the genus Pavlova. *Org. Geochem.* 15, 489–497. doi:10.1016/0146-6380(90)90094-G

Wang, H., Zhao, S. E., and Lin, Z. L. (2012). The key control factors and its petroleum and geological significance of extra-thick deposition in Dongying Formation, Nanpu Sag. *Earth Sci. Front.* 19 (1), 108–120.

Wang, X. Y., Jin, Z. K., Zhao, J. H., Zhu, Y., Hu, Z., Liu, G., et al. (2020). Depositional environment and organic matter accumulation of Lower Jurassic nonmarine fine-grained deposits in the Yuanba Area, Sichuan Basin, SW China. *Mar. Petroleum Geol.* 116, 104352. doi:10.1016/j.marpetgeo.2020.104352

Wei, W., and Algeo, T. J. (2019). Elemental proxies for paleosalinity analysis of ancient shales and mudrocks. *Geochem. Cosmochimica Acta* 287, 341–366. doi:10.1016/j.gca.2019.06.034

Wu, Z. R., He, S., He, Z. L., Li, X., Zhai, G., and Huang, Z. (2022). Petrographical and geochemical characterization of the Upper Permian Longtan formation and Dalong Formation in the Lower Yangtze region, South China: Implications for provenance, paleoclimate, paleoenvironment and organic matter accumulation mechanisms. *Mar. Petroleum Geol.* 139, 105580. doi:10.1016/j.marpetgeo.2022.105580

Xu, G., Hannah, J. L., Bingen, B., Georgiev, S., and Stein, H. J. (2012). Digestion methods for trace element measurements in shales: Paleoredox proxies examined. *Chem. Geol.* 324-325, 132–147. doi:10.1016/j.chemgeo.2012.01.029

Xu, S., Wang, Y. X., Bai, N., Wu, S., and Liu, B. (2024). Organic matter enrichment mechanism in saline lacustrine basins: A review. *Geol. J.* 59, 155–168. doi:10.1002/gj.4853

Yin, J., Xu, C. G., Hao, F., Wang, Q., Miao, Q., Wang, Z., et al. (2020). Controls on organic matter enrichment in source rocks of the Shahejie Formation in the southwestern Bozhong Sag, Bohai Bay Basin, China. *Palaeogeogr. Palaeoclimatol. Palaeoecol.* 560, 110026. doi:10.1016/j.palaeo.2020.110026

Yuan, W., Liu, G. D., Stebbins, A., Xu, L., Niu, X., Luo, W., et al. (2017). Reconstruction of redox Conditions during deposition of organic-rich shales of the Upper Triassic Yanchang Formation, Ordos basin, China. *Palaeogeogr. Palaeoclimatol. Palaeoecol.* 486, 158–170. doi:10.1016/j.palaeo.2016.12.020

Zhang, W. Z., Yang, W. W., and Xie, L. Q. (2017). Controls on organic matter accumulation in the Triassic Chang 7 lacustrine shale of the Ordos Basin, central China. *Int. J. Coal Geol.* 183, 38–51. doi:10.1016/j.coal.2017.09.015